

Highlights

Physics-informed spectral approximation of Koopman operators

Dimitrios Giannakis, Claire Valva

- New, spectrally accurate method to approximate Koopman operators from data.
- Makes direct use of equations of motion (physics).
- Extracts dynamically coherent observables under complex dynamics.
- Approximation can be computed from samples drawn from invariant measure, without need of time-ordered snapshots.
- Allows out-of-sample evaluation of eigenfunctions.

Physics-informed spectral approximation of Koopman operators

Dimitrios Giannakis^a, Claire Valva^b

^a*Department of Mathematics, Dartmouth College, 29 N. Main St., Hanover, 03755, New Hampshire, USA*

^b*Courant Institute of Mathematical Sciences, New York University, 251 Mercer St., New York, New York, 10012, USA*

Abstract

Koopman operators and transfer operators represent nonlinear dynamics in state space through its induced action on linear spaces of observables and measures, respectively. This framework enables the use of linear operator theory for supervised and unsupervised learning of nonlinear dynamical systems, and has received considerable interest in recent years. Here, we propose a data-driven technique for spectral approximation of Koopman operators of continuous-time, measure-preserving ergodic systems that is asymptotically consistent and makes direct use of known equations of motion (physics). Our approach is based on a bounded transformation of the Koopman generator (an operator implementing directional derivatives of observables along the dynamical flow), followed by smoothing by a Markov semigroup of kernel integral operators. This results in a skew-adjoint, compact operator whose eigendecomposition is expressible as a variational generalized eigenvalue problem. We develop Galerkin methods to solve this eigenvalue problem and study their asymptotic consistency in the large-data limit. A key aspect of these methods is that they are physics-informed, in the sense of making direct use of dynamical vector field information through automatic differentiation of kernel functions. Solutions of the eigenvalue problem reconstruct evolution operators that preserve unitarity of the underlying Koopman group while spectrally converging to it in a suitable limit. In addition, the computed eigenfunctions have representatives in a reproducing kernel Hilbert space, enabling out-of-sample evaluation of learned dynamical features. Numerical experiments performed with this method on integrable and chaotic low-dimensional systems demonstrate its efficacy in extracting dynamically coherent observables under complex dynamics.

Keywords:

Koopman operators, spectral approximation, data-driven techniques, kernel methods

1. Introduction

Dynamical systems can be characterized via an operator-theoretic formulation of ergodic theory through their induced action on linear spaces of observables, realized through Koopman (composition) operators and their duals, the Ruelle-Perron-Frobenius (transfer) operator [1, 2]. This framework allows one to translate problems of nonlinear dynamics, to equivalent linear, if infinite dimensional, problems about linear evolution operators which act on observables by composition with the flow map. As such, many relevant problems in the sciences, such as coherent feature extraction or statistical prediction can be formulated as linear problems. Starting from work in the late 1990s and early 2000s [3, 4, 5], the operator-theoretic approach has seen a surge of interest as a framework for data-driven techniques for analysis and modeling of dynamical systems [6, 7, 8, 9]. These methods have been successfully applied in diverse scientific domains, including fluid dynamics, climate dynamics, molecular dynamics, energy systems science, and control; see, for example, [10, 11, 12, 13, 14].

Despite the enticing theoretical properties of Koopman/transfer operators and recent progress in computational methodologies, the design of associated data-driven spectral approximation techniques is challenging. For example, a measure-preserving flow is weak-mixing if and only if the Koopman operator on L^2 has a simple eigenvalue at 1, with a constant corresponding eigenfunction, and no other eigenvalues [15]. Many commonly studied systems are rigorously known to be mixing, such as the Lorenz 63 (L63) system

[16, 17]. Further, even if the point spectrum of a dynamical system is nontrivial, it is not guaranteed to be discrete (e.g., the spectrum could possibly be dense in the unit circle). As such, to study systems with high dynamical complexity, numerical methods must be able to stably and consistently approximate the often non-discrete Koopman spectrum.

In scientific applications, it is additionally desirable to be able to use data-driven algorithms in combination with known physics to study a given system. Some popular and successful methods of this type include physics-informed neural networks [18] or physics-informed dynamic mode decomposition (piDMD) [19] that make use of structural information of a given dynamical system, e.g., enforcing that a fluid be incompressible or that the DMD modes are measure-preserving. Here, we will develop a method in this vein, where we make use of the equations of motion (i.e., known *physics*) from a given dynamical system time to approximate the spectrum of the Koopman generator.

Specifically, we propose a data-driven methodology for the approximation of Koopman and transfer operators in continuous-time measure-preserving ergodic flows that directly uses vector field information of the dynamical system, via the use of automatic differentiation of kernel functions. Our primary focus is the generator V of the unitary Koopman group $U^t = e^{tV}$ of such systems. The generator acts as a generalized derivative (detailed more in Section 2.1), i.e., $Vf = \lim_{t \rightarrow 0} \frac{U^t f - f}{t}$, and as such, if we have vector field data, we can directly compute the action of V upon a given function of sufficient regularity. We combine this observation with a bounded transformation of the Koopman generator and smoothing by kernel integral operators to build a family of skew-adjoint, unbounded operators $V_{z,\tau}$ with compact resolvents, parameterized by $z, \tau > 0$. The operators $V_{z,\tau}$ have purely discrete spectra by compactness of their resolvent and will be shown to converge spectrally to V in the iterated limit of $z \rightarrow 0^+$ after $\tau \rightarrow 0^+$ (see Theorem 6). Here, τ is a smoothing parameter and z will correspond to the smallest frequency scale the algorithm can faithfully resolve. We formulate the computation of eigenvalues and eigenvectors of $V_{z,\tau}$ as a variational generalized eigenvalue problem that admits well-posed Galerkin approximations in a learned basis of kernel eigenfunctions.

The eigendecomposition of $V_{z,\tau}$ then allows for the identification coherent features in a dynamical system through the eigenpairs (ω_j, ξ_j) , $V_{z,\tau} \xi_j = e^{i\omega_j \tau} \xi_j$, where $\xi_j \in L^2$ is the eigenfunction representing a coherent feature that evolves with characteristic frequency $\omega_j \in \mathbb{R}$. Additionally, each eigenfunction obtained via our scheme has a representative in a reproducing kernel Hilbert space (RKHS) of continuously differentiable functions. This enables out-of-sample evaluation to reconstruct eigenfunction time series at high temporal resolution from coarsely time-sampled (even independent) training data, among other supervised and unsupervised learning tasks.

In previous work, the authors have developed related techniques for spectral approximation of Koopman operators of measure-preserving ergodic flows which are based on compact approximations of the generator [20] or its resolvent [21]. Hereafter, we collectively reference these papers as DGV. The new contributions of this work, realized through explicit use of equations of motion, include:

1. Approximations of the Koopman generator and operator can be obtained from independent samples drawn from the invariant measure, rather than the time-ordered snapshots commonly used in DMD-type techniques.
2. Various discretization errors such as finite-difference approximation of the generator [20] or numerical quadrature for approximation of the resolvent [21] are avoided.
3. The use of automatic differentiation makes the scheme amenable to implementation using basis functions derived from eigendecomposition of general classes of kernel integral operators, including Markov smoothing operators adapted to the invariant measure.

We demonstrate our approach with numerical applications to low-dimensional dynamical systems exhibiting different types of spectral characteristics of the Koopman operator: an ergodic torus rotation, a Stepanoff flow on the 2-torus, and the L63 system on \mathbb{R}^3 . The examples illustrate the ability of our approach to stably compute eigenvalue and eigenfunctions of Koopman operators for systems that have them, and to identify slowly decorrelating observables that behave as approximate Koopman eigenfunctions under mixing dynamics.

The plan of the paper is as follows. In Section 2, we describe the dynamical system under study, along with our assumptions and function spaces employed in this work. In Sections 3 and 4, we describe our spectral approximation scheme and its numerical implementation, respectively. Section 5 presents our numerical experiments. Section 6 contains our primary conclusions and outlook on future work. Auxiliary technical results are collected in Appendix A. Appendix B summarizes the construction of variable-bandwidth kernels used in our numerical experiments.

2. Preliminaries and assumptions

2.1. Dynamical system

Our setup and notation follows closely DGV. In particular, we consider a continuous-time, continuous flow $\Phi^t: \mathcal{M} \rightarrow \mathcal{M}$, $t \in \mathbb{R}$, on a metric space \mathcal{M} , possessing an ergodic invariant Borel probability measure μ with compact support $X \subseteq \mathcal{M}$. We assume that there is a compact C^1 manifold $M \subseteq \mathcal{M}$ which is forward-invariant (i.e., $\Phi^t(M) \subseteq M$ for any $t \geq 0$) and contains X . These assumptions are met by many dynamical systems encountered in applications, including classes of measure-preserving flows on compact manifolds ($X = M = \mathcal{M}$), dissipative flows on manifolds with attractors ($X \subseteq M \subseteq \mathcal{M}$, with X being an attractor and M an absorbing set), and infinite-dimensional systems governed by dissipative partial differential equations with inertial manifolds.

The flow Φ^t induces a strongly-continuous group of unitary Koopman operators $U^t: H \rightarrow H$ that act on observables in the Hilbert space $H = L^2(\mu)$ by composition, $U^t f = f \circ \Phi^t$ [22, 23]. Moreover, the adjoint of the Koopman operator $U^{t*} \equiv U^{-t}$ is the transfer operator that governs the evolution of densities of measures in H under the dynamics. By Stone's theorem on strongly continuous, one-parameter unitary groups [24], the Koopman group $\{U^t\}_{t \in \mathbb{R}}$ has a skew-adjoint generator $V: D(V) \rightarrow H$, defined on a dense subspace $D(V) \subseteq H$ by means of the norm limit

$$Vf = \lim_{t \rightarrow 0} \frac{U^t f - f}{t}.$$

The generator V completely characterizes the Koopman group, in the sense that if two strongly continuous, one-parameter unitary groups have the same generator V they are identical [25]. Moreover, V reconstructs the Koopman operator at any time $t \in \mathbb{R}$ by exponentiation, $U^t = e^{tV}$, defined via the Borel functional calculus.

When acting on elements with continuously differentiable representatives in $C^1(M)$, V reduces to a directional derivative along the vector field $\vec{V}: M \rightarrow TM$ that generates Φ^t . Specifically, we have

$$V \iota f = \iota \vec{V} \cdot \nabla f, \quad f \in C^1(M), \quad (1)$$

where $\iota: C(M) \rightarrow H$ is the map that sends continuous functions on M to their corresponding equivalence classes in H , and the vector field \vec{V} satisfies

$$\frac{d}{dt} \Phi^t(x) = \vec{V}(\Phi^t(x)), \quad x \in M. \quad (2)$$

In other words, \vec{V} represents the equations of motion (“physics”) governing the flow. In this work, we assume that the vector field \vec{V} is known to us in the form of governing equations for the initial-value problem (2).

In the following, we write $\langle f, g \rangle = \int_X f^* g d\mu$ and $\|f\|_H = \langle f, f \rangle$ for the inner product and norm of H , respectively, where the inner product is taken conjugate-linear in the first argument. Moreover, $\mathbf{1}: \mathcal{M} \rightarrow \mathbb{R}$ is the function on \mathcal{M} equal to 1 everywhere. We will denote the space of bounded linear maps between Banach spaces \mathbb{E} and \mathbb{F} as $B(\mathbb{E}, \mathbb{F})$, and $\|A\|$ will be the operator norm of $A \in B(\mathbb{E}, \mathbb{F})$. We will use the abbreviation $B(\mathbb{E}) \equiv B(\mathbb{E}, \mathbb{E})$. Given an operator $A: D(A) \rightarrow \mathbb{E}$ defined on a subspace $D(A) \subseteq \mathbb{E}$, $\rho(A)$ and $\sigma(A)$ will denote the resolvent set and spectrum of A , respectively. For a complex number $z \in \rho(A)$, $R(z, A) \in B(\mathbb{E})$ will be the corresponding resolvent operator, $R(z, A) = (z - V)^{-1}$. Note that for $z \in \rho(A)$, $z - V$ is a surjective operator.

2.2. Spectral decomposition

Our objective is to approximate the generator V from Section 2.1 by a family of operators whose spectral properties are amenable to numerical approximation, while also providing dynamically relevant feature extraction. Importantly, we seek that our approximations are physics-informed, in the sense of making use of the known dynamical vector field \vec{V} via (1). In this subsection, we give a brief outline of results from spectral theory that underpin our constructions. For detailed expositions of these topics see, e.g., [1, 2, 26, 25].

By the spectral theorem for skew-adjoint operators, the spectrum $\sigma(V)$ of the generator V is a closed subset of the imaginary line, and there exists a projection-valued measure (PVM) $E: \mathcal{B}(i\mathbb{R}) \rightarrow B(H)$ on the Borel σ -algebra $\mathcal{B}(i\mathbb{R})$ of the imaginary line that decomposes the generator and Koopman operators via the spectral integrals

$$V = \int_{i\mathbb{R}} i\omega dE(i\omega), \quad U^t = \int_{i\mathbb{R}} e^{i\omega t} dE(i\omega). \quad (3)$$

Moreover, there is a U^t -invariant splitting $H = H_p \oplus H_c$ into orthogonal subspaces H_p and H_c such that the spectral measure $E_p: \mathcal{B}(i\mathbb{R}) \rightarrow B(H_p)$ of $V|_{H_p}$ is discrete and the spectral measure $E_c: \mathcal{B}(i\mathbb{R}) \rightarrow B(H_c)$ of $V|_{H_c}$ is purely continuous (i.e., has no atoms), yielding the decomposition $E = E_p \oplus E_c$.

The atoms of E_p are singleton sets $\{i\omega_j\}$ containing the eigenvalues of V ,

$$V\xi_j = i\omega_j\xi_j, \quad \omega_j \in \mathbb{R}, \quad \xi_j \in H_p \setminus \{0\},$$

and the corresponding eigenfunctions ξ_j form an orthonormal basis of H_p . By (3), we have $U^t\xi_j = e^{i\omega_j t}\xi_j$, so ξ_j has periodic evolution with period $2\pi/\omega_j$. We therefore interpret the real numbers ω_j as eigenfrequencies of the dynamical system. It can be shown that, by ergodicity, the eigenvalues of V are all simple, and, by definition of V , come in complex-conjugate pairs. We can therefore choose a \mathbb{Z} -based indexing such that $\omega_0 = 1$, $\xi_0 = \mathbf{1}$, and $\omega_{-j} = -\omega_j$, $\xi_{-j} = -\xi_j^*$ for $j \neq 0$. It can further be shown that the eigenfunctions ξ_j lie in $L^\infty(\mu)$ with $|\xi_j| = 1$ μ -a.e. when ξ_j is normalized to unit $L^2(\mu)$ norm, and they form a multiplicative group, $\xi_j\xi_k = \xi_l$, with the eigenfrequencies forming an additive group, $\omega_j + \omega_k = \omega_l$.

Based on the above, a collection $\xi_{j_1}, \dots, \xi_{j_d}$ of eigenfunctions induces a feature map $F: \mathcal{M} \rightarrow \mathbb{C}^d$, where $F(x) = (\xi_{j_1}(x), \dots, \xi_{j_d}(x))$ μ -a.e. and the range of F is a subset of the d -dimensional torus $\mathbb{T}^d \subset \mathbb{C}^d$. A key property of this feature map is that it intertwines the dynamics on \mathcal{M} with a rotation system $R^t: \mathbb{T}^d \rightarrow \mathbb{T}^d$ parameterized by the eigenfrequencies corresponding to $\xi_{j_1}, \dots, \xi_{j_d}$; that is, we have $R^t \circ F(x) = F \circ \Phi^t(x)$, μ -a.e., where $R^t(\theta) = \theta + \alpha t \bmod 2\pi$ and $\alpha = (\omega_{j_1}, \dots, \omega_{j_d})$. Such a map F is called a measure-theoretic semiconjugacy, and it is called a topological semiconjugacy if the functions $\xi_{j_1}, \dots, \xi_{j_d}$ are continuous. In addition, the existence of the Koopman eigenfunction basis of H_p leads to a closed-form expression for the dynamical evolution of observables in this space,

$$U^t f = \sum_j \langle \xi_j, f \rangle e^{i\omega_j t} \xi_j, \quad \forall f \in H_p, \quad (4)$$

which can be used to build predictive models when coupled with methods for estimating the expansion coefficients $\langle \xi_j, f \rangle$. Defining the cross-correlation function of two observables $f, g \in H$ as $C_{fg}(t) = \langle f, U^t g \rangle$, it follows from (4) that $C_{fg}(t) = \sum_j \langle g, \xi_j \rangle e^{i\omega_j t} \langle \xi_j, f \rangle$ has a quasiperiodic evolution that does not decay to 0 as $t \rightarrow \infty$ whenever $f, g \in H_p$. This suggests the possibility of long-term predictability of observables in this space.

In contrast to the structured nature of the Koopman spectra and evolution of observables in H_p , observables in the continuous spectrum subspace H_c are characterized by a decay of correlations which is characteristic of weak-mixing dynamics, $\lim_{T \rightarrow \infty} \int_0^T |C_{fg}(t)| dt / T = 0$ for all $f \in H$ and $g \in H_c$. In particular, there is no basis of H_c compatible with the evolution of observables analogously to the Koopman eigenfunction basis of H_p , and this poses a significant methodological obstacle when dealing with observables in H that are not well-approximated by elements of H_p . Indeed, by fundamental results from ergodic theory, the flow Φ^t is weak-mixing if and only if H_p is the one-dimensional subspace of H spanned by constant functions. If we consider mixing a hallmark of high dynamical complexity in a measure-theoretic sense,

this suggests that in many real-world problems feature extraction and prediction based purely on Koopman eigenfunctions in H will perform poorly.

To overcome these obstacles, considerable efforts have been made in recent years to develop techniques capable of consistently approximating the continuous spectra of unitary Koopman operators induced from measure-preserving dynamics; see, e.g., [8, 9] for surveys. Building on DGV, the approach taken in this paper will be to approximate V by a family of skew-adjoint operators that are diagonalizable on the entire Hilbert space H , and converge to V in a spectral sense. In the next subsection, we lay out the notions of spectral convergence employed for that purpose.

2.3. Spectral convergence

We will use the following notions of the convergence of skew-adjoint operators [27, 26].

Definition 1 (Convergence of skew-adjoint operators). Let $A: D(A) \rightarrow \mathbb{H}$ be a skew-adjoint operator on a Hilbert space \mathbb{H} and $A_\tau: D(A_\tau) \rightarrow \mathbb{H}$ a family of skew-adjoint operators indexed by $\tau > 0$.

- (i) The family A_τ is said to converge in strong resolvent sense to A as $\tau \rightarrow 0^+$, denoted $A_\tau \xrightarrow{\text{sr}} A$, if for some (and thus, every) $z \in \mathbb{C} \setminus i\mathbb{R}$ the resolvents $R(z, A_\tau)$ converge strongly to $R(z, A)$; that is, $\lim_{\tau \rightarrow 0^+} R(z, A_\tau)f = R(z, A)f$ for every $f \in \mathbb{H}$.
- (ii) The family A_τ is said to converge in strong dynamical sense to A as $\tau \rightarrow 0^+$, denoted $A_\tau \xrightarrow{\text{sd}} A$ if, for every $t \in \mathbb{R}$, the unitary operators e^{tA_τ} converge strongly to e^{tA} ; that is, $\lim_{\tau \rightarrow 0^+} e^{tA_\tau}f = e^{tA}f$ for every $f \in \mathbb{H}$.

It can be shown, [e.g., 26, Proposition 10.1.8], that strong resolvent convergence and strong dynamical convergence are equivalent notions. For our purposes, this implies that if a family of skew-adjoint operators converges to the Koopman generator V in strong resolvent sense, the unitary evolution groups generated by these operators consistently approximate the Koopman group generated by V .

Strong resolvent convergence and strong dynamical convergence imply the following form of spectral convergence [e.g., 20, Proposition 13].

Theorem 2. With the notation of Definition 1, let $\tilde{E}: \mathcal{B}(i\mathbb{R}) \rightarrow B(\mathbb{H})$ and $\tilde{E}_\tau: \mathcal{B}(i\mathbb{R}) \rightarrow B(\mathbb{H})$ be the spectral measures of A and A_τ , respectively, i.e., $A = \int_{i\mathbb{R}} \lambda d\tilde{E}(\lambda)$ and $A_\tau = \int_{i\mathbb{R}} \lambda d\tilde{E}_\tau(\lambda)$. Then, the following hold under strong resolvent convergence of A_τ to A .

- (i) For every element $\lambda \in \sigma(A)$ of the spectrum of A , there exists a sequence $\tau_1, \tau_2, \dots \searrow 0$ and elements $\lambda_n \in \sigma(A_{\tau_n})$ of the spectra of A_{τ_n} such that $\lim_{n \rightarrow \infty} \lambda_n = \lambda$.
- (ii) For every bounded continuous function $h: i\mathbb{R} \rightarrow \mathbb{C}$, as $\tau \rightarrow 0^+$ the operators $h(A_\tau) = \int_{i\mathbb{R}} h(\lambda) d\tilde{E}_\tau(\lambda)$ converge strongly to $h(A) = \int_{i\mathbb{R}} h(\lambda) d\tilde{E}(\lambda)$.
- (iii) For every bounded Borel-measurable set $\Theta \in \mathcal{B}(i\mathbb{R})$ such that $\tilde{E}(\partial\Theta) = 0$ (i.e., the boundary of Θ does not contain eigenvalues of A_τ), as $\tau \rightarrow 0^+$ the projections $\tilde{E}_\tau(\Theta)$ converge strongly to $\tilde{E}(\Theta)$.

2.4. Markov smoothing operators

We will regularize the generator V by pre- and post-composing it with kernel integral operators G_τ that converge strongly to the identity as $\tau \rightarrow 0^+$. These operators are induced from a family of kernel functions $p_\tau: \mathcal{M} \times \mathcal{M} \rightarrow \mathbb{R}$, $\tau > 0$, with the following properties.

- (K1) p_τ is measurable, and it is continuously differentiable on $M \times M$.
- (K2) p_τ is Markovian with respect to μ ; i.e., $p_\tau \geq 0$ and for every $x \in \mathcal{M}$ the normalization condition $\int_X p_\tau(x, \cdot) d\mu = 1$ holds.

For every such kernel function p_τ , we let $G_\tau: H \rightarrow H$ be the corresponding integral operator on H with

$$G_\tau f = \int_X p_\tau(\cdot, x) f(x) d\mu(x). \quad (5)$$

We then require that the following hold.

(K3) The family $\{G_\tau: H \rightarrow H\}_{\tau>0} \cup \{G_0: = \text{Id}\}$ forms a strongly continuous semigroup; i.e., $G_\tau G_{\tau'} = G_{\tau+\tau'}$ for every $\tau, \tau' \geq 0$ and $\lim_{\tau \rightarrow 0^+} G_\tau f = f$ for every $f \in H$.

(K4) G_τ is strictly positive; i.e., $\langle f, G_\tau f \rangle > 0$ for every nonzero $f \in H$.

(K5) G_τ is ergodic; i.e., $G_\tau f = f$ for all $\tau > 0$ iff f is constant μ -a.e.

Note that every such kernel p_τ is necessarily symmetric, $p_\tau(x, y) = p_\tau(y, x)$, and the corresponding integral operator G_τ is self-adjoint and of trace class.

Let $k: \mathcal{M} \times \mathcal{M} \rightarrow \mathbb{R}_+$ be a positive measurable kernel function that is continuously differentiable and integrally strictly positive definite on $M \times M$. The latter requirement means [28] that for every finite Borel measure ν on \mathcal{M} with support contained in M we have

$$\int_M \int_M k(x, y) d\nu(x) d\nu(y) > 0. \quad (6)$$

Following DGV, we use such a kernel k to build the family p_τ by first constructing a symmetric Markov kernel $p: \mathcal{M} \times \mathcal{M} \rightarrow \mathbb{R}$ by means of a bistochastic kernel normalization procedure proposed by [29], and adapted for the purposes of this work. The normalization procedure involves computing the continuous functions $d, q \in C^1(M)$ and the asymmetric kernel function $\hat{k}: \mathcal{M} \times \mathcal{M} \rightarrow \mathbb{R}$ defined as

$$d = \int_M k(\cdot, x) d\mu(x), \quad q = \int_M \frac{k(\cdot, x)}{d(x)} d\mu(x), \quad \hat{k}(x, y) = \frac{k(x, y)}{d(x)q^{1/2}(y)}. \quad (7)$$

We then set

$$p(x, y) = \int_X \hat{k}(x, z) \hat{k}(z, y) d\mu(z). \quad (8)$$

One can readily verify that $p(x, y) > 0$, $p(x, y) = p(y, x)$, and $\int_X p(x, \cdot) d\mu = 1$ for every $x, y \in M$; that is, p is a strictly positive Markovian kernel. Moreover, by compactness of X , the restriction of p on $M \times M$ is C^1 .

Consider now the integral operator $\hat{K}: H \rightarrow C^1(M)$, where

$$\hat{K}f = \int_M \hat{k}(\cdot, x) f(x) d\mu(x),$$

and define $\tilde{K}: H \rightarrow H$ and $G: H \rightarrow H$ as $\tilde{K} = \iota \hat{K}$, $G = \tilde{K} \tilde{K}^*$. Observe that G is a kernel integral operator with kernel p ,

$$Gf = \int_X p(\cdot, x) f(x) d\mu(x),$$

and by Markovianity and continuity of p , G is a self-adjoint Markov operator of trace class. Moreover, by (6), G is a strictly positive operator, and thus admits an eigendecomposition

$$G\phi_j = \lambda_j \phi_j,$$

where $j \in \mathbb{N}_0$, the ϕ_j form an orthonormal basis of H , and the eigenvalues λ_j are strictly positive and have finite multiplicities. By convention, we order the eigenvalues λ_j in decreasing order, so that $\lambda_0 = 1$ by Markovianity. It also follows by strict positivity of k and compactness of X that the Markov process generated by G is ergodic. This means that λ_0 is a simple eigenvalue, and the corresponding eigenfunction ϕ_0 can be chosen as being μ -a.e. equal to 1.

For the purposes of the physics-informed approximation schemes studied in this paper, it is important that (i) the eigenfunctions ϕ_j have representatives in $C^1(M)$; and (ii) directional derivatives of these representatives can be computed by taking derivatives of the kernel functions \hat{k} . First, observe that an eigen-decomposition of G can be obtained from a singular value decomposition (SVD) of the compact operator \tilde{K} ,

$$\tilde{K} = \sum_{j=0}^{\infty} \phi_j \sigma_j \langle \gamma_j, \cdot \rangle,$$

where ϕ_j (resp. γ_j) are left (resp. right) singular vectors forming an orthonormal basis of H , and $\sigma_j = \lambda_j^{1/2}$ are strictly positive singular values. One finds that the functions

$$\varphi_j = \frac{1}{\sigma_j} \hat{K} \gamma_j \quad (9)$$

are representatives of ϕ_j in $C^1(M)$; that is, $\phi_j = \iota \varphi_j$ which implies that ϕ_j lies in $D(V)$. As a result, using (1), we can compute the action of the generator on the eigenbasis as

$$V \phi_j = \iota \vec{V} \cdot \nabla \varphi_j \equiv \tilde{K}' \gamma_j, \quad (10)$$

where $\tilde{K}' = \iota \hat{K}'$ and $\hat{K}': H \rightarrow C(M)$ is the integral operator

$$\hat{K}' f = \int_X \hat{k}'(\cdot, y) f(y) d\mu(y), \quad \hat{k}'(\cdot, y) = \vec{V} \cdot \nabla \hat{k}(\cdot, y).$$

We therefore see that $V \phi_j$ can be computed from the right singular vectors γ_j so long as the directional derivatives $\hat{k}'(\cdot, y)$ of the kernel sections $\hat{k}(\cdot, y)$ along \vec{V} are known. For later convenience, we set $\phi'_j = V \phi_j$ and $\varphi'_j = \vec{V} \cdot \nabla \varphi_j$.

Finally, to build the Markov semigroup G_τ , we define the self-adjoint operator $\Delta: D(\Delta) \rightarrow H$ on the dense domain $D(\Delta) = \{f \in H : \sum_{j=1}^{\infty} \eta_j^2 |\langle \phi_j, f \rangle|^2 < \infty\}$ via the eigendecomposition

$$\Delta \phi_j = \eta_j \phi_j, \quad \eta_j = \frac{\lambda_j^{-1} - 1}{\lambda_1^{-1} - 1}.$$

Intuitively, we think of Δ as a Laplace-type operator, and we will use it as the generator of our Markov semigroup,

$$G_\tau = e^{-\tau \Delta}, \quad \tau \geq 0.$$

In [20, Theorem 1], it is shown that for each $\tau > 0$, G_τ is a Markovian kernel integral operator of the form (5), with kernel $p_\tau \in C^1(M \times M)$ given by a Mercer sum,

$$p_\tau(x, y) = \sum_{j=0}^{\infty} \lambda_{j,\tau} \varphi_j(x) \varphi_j(y), \quad \lambda_{j,\tau} = e^{-\tau \eta_j},$$

that converges in $C^1(M \times M)$ norm. In particular, the kernels p_τ satisfy all the requisite properties (K1)–(K5) listed above. Moreover, building the semigroup G_τ from the generator Δ means that the eigenvalues/eigenvectors of G_τ can be directly obtained from eigenvalues/eigenvectors of G . This will be useful in Section 4 for developing (data-driven) Galerkin methods.

2.5. Reproducing kernel Hilbert spaces

We outline a few results from RKHS theory used in our spectral approximation scheme. Further details on these constructions and terminology can be found in [20]. Comprehensive expositions on RKHSs are available, e.g., in [30, 31].

Lemma 3. *Let $\kappa: M \times M \rightarrow \mathbb{R}$ be a positive-definite, Borel-measurable kernel function. Then, for every finite Borel measure ν on M with (compact) support X_ν , the kernel $\kappa_2: M \times M \rightarrow \mathbb{R}$ defined as $\kappa_2(x, y) = \int_M \kappa(x, z)\kappa(z, y) d\nu(z)$ is positive definite. Moreover, if κ is strictly positive-definite on X_ν , then so is κ_2 .*

Proof. See [20, Lemma 12]. \square

Next, observe that the kernel p from (8) can be expressed as

$$p(x, y) = \int_M \frac{\tilde{k}(x, z)\tilde{k}(z, y)}{\tilde{d}(x)\tilde{d}(z)} d\mu(z), \quad \tilde{k}(x, y) = \frac{k(x, y)}{q^{1/2}(x)q^{1/2}(y)}, \quad \tilde{d}(x) = \frac{d(x)}{q^{1/2}(x)}.$$

By strict positivity of the kernel k , \tilde{d} and q are strictly positive, continuous functions, and thus bounded away from zero on the compact set M . As a result, since k is integrally strictly positive so is \tilde{k} . Moreover, by Lemma 3, $(x, y) \mapsto \int_M \tilde{k}(x, z)\tilde{k}(z, y) d\mu(z)$ is positive-definite on M and strictly positive-definite on X_ν , and p inherits these properties by strict positivity of \tilde{d} . Similarly to p_τ , p has a Mercer expansion,

$$p(x, y) = \sum_{j=0}^{\infty} \lambda_j \varphi_j(x) \varphi_j(y),$$

which converges in $C^1(M \times M)$ norm.

Let $\mathcal{H} \subset C^1(M)$ be the RKHS on M with reproducing kernel p . We denote the inner product of \mathcal{H} by $\langle \cdot, \cdot \rangle_{\mathcal{H}}$. For a subset $S \subseteq M$ we define the Hilbert subspace $\mathcal{H}(S) \subseteq \mathcal{H}$ as $\mathcal{H}(S) = \overline{\text{span}\{p(x, \cdot) : x \in S\}}^{\|\cdot\|_{\mathcal{H}}}$. This space can be identified with the restriction $\mathcal{H}|_S \subseteq C(S)$ of \mathcal{H} onto S . By strict positivity of the λ_j , $\mathcal{H}(X)$ can thus be identified with a dense subspace of $C(X)$. Moreover, $H^1 := \iota\mathcal{H}$ is a dense subspace of H and the embedding $\mathcal{H}(X) \hookrightarrow H$ is compact. The subspace H^1 can be equivalently characterized by a decay condition of expansion coefficients of elements of H with respect to the ϕ_j basis,

$$H^1 = \left\{ f \in H : \sum_{j=0}^{\infty} \frac{|\langle \phi_j, f \rangle|^2}{\lambda_j} < \infty \right\},$$

and becomes a Hilbert space for the inner product $\langle f, g \rangle_{H^1} = \sum_{j=0}^{\infty} \lambda_j^{-1} \langle f, \phi_j \rangle \langle \phi_j, g \rangle$. Note that, as a vector space, H^1 is equal to the domain of $G^{-1/2}$, and

$$\|f\|_{H^1} = \|G^{-1/2}f\|_H \geq \|f\|_H$$

holds since G is a contraction. Moreover, H^1 is a subspace of $D(V)$ and, by exponential decay of $\lambda_{j,\tau}$ with increasing η_j , contains $\text{ran } G_\tau$ as a subspace for all $\tau > 0$. In particular, $G^{-1/2}G_\tau$ is a bounded operator on H for every $\tau > 0$.

Using standard RKHS constructions (see, e.g., [20, Section 4.1]), it can be shown that $P: H \rightarrow \mathcal{H}$ with

$$Pf = \int_X p(\cdot, x) f(x) d\mu(x)$$

is a well-defined, Hilbert–Schmidt operator, whose range is a dense subspace of $\mathcal{H}(X)$. Moreover, the adjoint $P^*: \mathcal{H} \rightarrow H$ maps functions in \mathcal{H} to their corresponding equivalence classes in H (i.e., $P^*f = \iota f$), leads to the factorization $G = P^*P$ of the Markov integral operator G from Section 2.4. Using these facts, we can deduce the following polar decomposition of P ,

$$P = TG^{1/2}, \tag{11}$$

where $T: H \rightarrow \mathcal{H}$ is an isometry with $\text{ran } T = \mathcal{H}(X)$. Moreover, the functions $\psi_j := \lambda_j^{1/2} \varphi_j$, $j \in \mathbb{N}_0$, form an orthonormal basis of $\mathcal{H}(X)$, while $\{\phi_j^{(1)} := \iota \psi_j\}_{j \in \mathbb{N}_0}$ is an orthonormal basis of H^1 . By (11), we have $P^*T = G^{1/2}$. This implies that

$$Tf = \sum_{j=0}^{\infty} \langle \phi_j, f \rangle \psi_j, \tag{12}$$

and thus that the L^2 element $\iota T f = P^* T f$ has basis expansion $\iota T f = \sum_{j=0}^{\infty} \lambda_j^{1/2} \langle \phi_j, f \rangle \phi_j$. Since $\lambda_j < 1$ for all $j \in \mathbb{N}$, we can interpret T as a smoothing operator even though it is unitary as a map from H to $\mathcal{H}(X)$. Later on, we will make use of a truncated version $T_{L'}: H \rightarrow \mathcal{H}$ of T , defined for $L' \in \mathbb{N}_0$ as

$$T_{L'} f = \sum_{j=0}^{L'} \langle \phi_j, f \rangle \psi_j. \quad (13)$$

These operators are partial isometries that converge strongly to T as $L' \rightarrow \infty$.

Next, the Nyström operator $\mathcal{N}: D(\mathcal{N}) \rightarrow \mathcal{H}$ is an unbounded operator with dense domain $D(\mathcal{N}) = H^1 \subseteq H$ and range $\mathcal{H}(X)$ that maps elements in its domain to their representatives in $\mathcal{H}(X)$ according to the formula

$$\mathcal{N} f = \sum_{j=0}^{\infty} \frac{\langle \phi_j, f \rangle}{\lambda_j^{1/2}} \psi_j. \quad (14)$$

This induces in turn a Dirichlet energy functional $\mathcal{E}: H^1 \rightarrow \mathbb{R}$ that provides a measure of average spatial variability of elements in its domain with respect to the RKHS \mathcal{H} ,

$$\mathcal{E}(f) = \frac{\|\mathcal{N} f\|_{\mathcal{H}}^2}{\|f\|_H^2} - 1.$$

Note that $\mathcal{E}(f) \geq 0$ with equality iff f is constant μ -a.e.

Remark 4. When implemented using the pullback of a kernel $k^{(Y)}$ on data space Y under a map $F: \mathcal{M} \rightarrow Y$, the isometric embedding (12) and Nyström extension (14) are pullbacks of everywhere-defined functions on Y , i.e., $T f = g \circ F$ and $\mathcal{N} f = h \circ F$ with $g, h: Y \rightarrow \mathbb{R}$. In the case of the bistochastic kernel construction described in Section 2.4, these functions are given by

$$g = \sum_{j=0}^{\infty} \langle \phi_j, f \rangle \psi_j^{(Y)}, \quad h = \sum_{j=0}^{\infty} \frac{\langle \phi_j, f \rangle}{\sigma_j} \psi_j^{(Y)},$$

where $\psi_j^{(Y)} = \int_M \hat{k}^{(Y)}(\cdot, F(x)) \gamma_j(x) d\mu(x)$. Here, $\hat{k}^{(Y)}: Y \times Y \rightarrow \mathbb{R}$ is the kernel on data space obtained by normalization of $k^{(Y)}$ using analogous steps to (7).

To verify well-posedness of our spectral approximation scheme, we will also need the space of distributions $H^{-1} := (H^1)^*$ given by the continuous dual of H^1 as a subspace of H . Since H is a self-dual space, it can be identified with a subspace of H^{-1} , leading to the triple

$$H^1 \subset H \subset H^{-1}.$$

By Hilbert space duality we also have that H^{-1} is a Hilbert space with orthonormal basis $\{\phi_j^{(-1)} := \lambda_j^{-1/2} \phi_j\}$. In particular, the action of a distribution $\alpha = \sum_{j=0}^{\infty} a_j \phi_j^{(-1)} \in H^{-1}$ on an observable $f = \sum_{j=0}^{\infty} c_j \phi_j^{(1)} \in H^1$ is given by $\alpha f = \sum_{j=0}^{\infty} a_j c_j$. It follows from the fact that λ_j decays to 0 as $j \rightarrow \infty$ with no accumulation points other than 0 that the embeddings $H^1 \hookrightarrow H$ and $H \hookrightarrow H^{-1}$ are both compact.

3. Spectral approximation scheme

In what follows, we will build a family of densely-defined operators $V_{z,\tau}: D(V_{z,\tau}) \rightarrow H$, $D(V_{z,\tau}) \subseteq H$, parameterized by $z, \tau > 0$ with the following properties.

- (P1) $V_{z,\tau}$ is skew-adjoint.
- (P2) $V_{z,\tau}$ has compact resolvent.
- (P3) $V_{z,\tau}$ is real, $(V_{z,\tau} f)^* = V_{z,\tau}(f^*)$ for all $f \in D(V)$.

(P4) $V_{z,\tau}$ annihilates constant functions, $V_{z,\tau}\mathbf{1} = 0$.

(P5) $V_{z,\tau} \xrightarrow{\text{sr}} V$ in the iterated limits $z \rightarrow 0^+$ after $\tau \rightarrow 0^+$.

In the above, τ is the kernel smoothing parameter introduced in Section 2.4, used here to effect compactification of the resolvent. Moreover, as we will see momentarily, the parameter z can be intuitively thought of as controlling the approximate “invertibility” of a bounded transformation applied to V prior to compactification.

Let $\tilde{H} = \{f \in H : \langle \mathbf{1}, f \rangle = 0\}$ be the closed subspace of H consisting of zero-mean functions with respect to the invariant measure μ . Let also $\Pi_0 = \langle \mathbf{1}, \cdot \rangle_H$ and $\tilde{\Pi} = \text{Id} - \Pi_0$, where $\tilde{\Pi}$ is the orthogonal projection onto \tilde{H} . Since $V\mathbf{1} = 0$, \tilde{H} is an invariant subspace of V . To construct $V_{z,\tau}$, we begin by considering a bounded, skew-adjoint transformation of the generator, obtained from the bounded, continuous, antisymmetric function $q_z : i\mathbb{R} \rightarrow \mathbb{C}$,

$$q_z(i\omega) = \frac{i\omega}{z^2 + \omega^2}, \quad \text{ran } q_z = i \left[-\frac{1}{2z}, \frac{1}{2z} \right], \quad (15)$$

via the Borel functional calculus:

$$Q_z := q_z(V|_{\tilde{H}}) \equiv R_z^* V R_z, \quad Q_z \in B(\tilde{H}), \quad Q_z^* = -Q_z,$$

where $R_z = R(z, V)$. Note that above (and in what follows when convenient) we consider V and R_z as operators on \tilde{H} .

The function q_z is plotted in Fig. 1. While it is not invertible, its restriction \tilde{q}_z on the subset $i\Omega_z := i(-\infty, -z] \cup i[z, \infty)$ of the imaginary line is invertible, with inverse $\tilde{q}_z^{-1} : i[-(2z)^{-1}, (2z)^{-1}] \setminus \{0\} \rightarrow i\mathbb{R}$,

$$\tilde{q}_z^{-1}(i\omega) = i \frac{1 + \sqrt{1 - 4z^2\omega^2}}{2\omega}. \quad (16)$$

As a result, $\tilde{V}_z := \tilde{q}_z^{-1}(Q_z)$ is a skew-adjoint operator with dense domain $D(\tilde{V}_z) \subset \tilde{H}$ that reconstructs the generator V on the spectral domain Ω_z . We extend \tilde{V}_z to the full Hilbert space H by defining $V_z = \tilde{\Pi}\tilde{V}_z\tilde{\Pi}$. The value of z controls the approximate invertibility of the function q_z , as values in $i(-z, z) \setminus \{0\}$ will be mapped to the “wrong” value under \tilde{q}_z^{-1} . This intuition informs the $z \rightarrow 0^+$ limit, which is made precise in Theorem 5 below. This result is central to our scheme as it allows approximating the generator in a spectral sense using the bounded, skew-adjoint operators Q_z .

Theorem 5. *As $z \rightarrow 0^+$, V_z converges to V in strong resolvent sense. As a result, it converges to V in strong dynamical sense, $e^{tV_z} \xrightarrow{\text{sd}} U^t$, and it converges spectrally in the sense of Theorem 2.*

Proof. Recall the spectral resolution of V in (3), $V = \int_{i\mathbb{R}} i\omega dE(i\omega)$, and define the PVM $\tilde{E} : \mathcal{B}(i\mathbb{R}) \rightarrow B(\tilde{H})$ as $\tilde{E} = \tilde{\Pi} \circ E$. Note that \tilde{E} does not have an atom at 0 (i.e., $\tilde{E}(\{0\}) = 0$) and $V|_{\tilde{H}} = \int_{i\mathbb{R}} i\omega d\tilde{E}(i\omega)$. For $y > 0$, we also define the resolvent function $r_y : i\mathbb{R} \rightarrow \mathbb{C}$ as $r_y(i\omega) = 1/(y - i\omega)$, so that $R(y, A) = r_y(A)$ for any skew-adjoint operator A .

We then have that

$$R(y, \tilde{V}_z) = r_y(\tilde{V}_z) = r_y(\tilde{q}_z^{-1}(q_z(V|_{\tilde{H}}))) = \int_{i\mathbb{R}} r_y(\tilde{q}_z^{-1}(q_z(i\omega))) d\tilde{E}(i\omega),$$

giving

$$\begin{aligned} R(y, \tilde{V}_z) &= \int_{i\Omega_z} r_y(\tilde{q}_z^{-1}(q_z(i\omega))) d\tilde{E}(i\omega) + \int_{-z}^z r_y(\tilde{q}_z^{-1}(q_z(i\omega))) d\tilde{E}(i\omega) \\ &= \int_{i\Omega_z} r_y(i\omega) d\tilde{E}(i\omega) + \int_{-z}^z r_y(i\omega) d\tilde{E}(i\omega) - \int_{-z}^z r_y(i\omega) d\tilde{E}(i\omega) + \int_{-z}^z r_y(\tilde{q}_z^{-1}(q_z(i\omega))) d\tilde{E}(i\omega) \\ &= R(y, V|_{\tilde{H}}) - \int_{-z}^z r_y(i\omega) d\tilde{E}(i\omega) + \int_{-z}^z r_y(\tilde{q}_z^{-1}(q_z(i\omega))) d\tilde{E}(i\omega) \end{aligned} \quad (17)$$

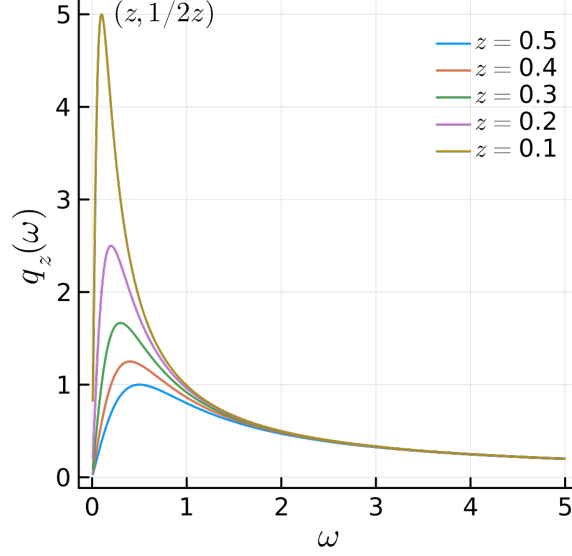


Figure 1: Graphs of the transformation function q_z for the generator for representative values of z .

We will prove the strong resolvent convergence $\tilde{V}_z \xrightarrow{\text{sr}} V|_{\tilde{H}}$ by showing that the two rightmost terms of (17) converge strongly to zero on \tilde{H} .

For $\omega \in (-z, z) \setminus \{0\}$,

$$\tilde{q}_z^{-1}(q_z(i\omega)) = \tilde{q}_z^{-1}\left(\frac{i\omega}{z^4 + \omega^2}\right) = iz^2/\omega,$$

so we have

$$|r_y(\tilde{q}_z^{-1}(q_z(i\omega)))| = \left|\frac{1}{y - z^2/\omega}\right| = \left(y^2 + \frac{z^2}{\omega^2}\right)^{-1/2} \leq \frac{1}{y}.$$

Similarly, $|r_y(i\omega)| < 1/y$.

Next, for $f \in \tilde{H}$, let $\tilde{E}_f: \mathcal{B}(i\mathbb{R}) \rightarrow \mathbb{R}_+$ be the positive finite Borel measure given by $\tilde{E}_f(\Omega) = \langle f, \tilde{E}(\Omega)f \rangle$. Using the above upper bounds for $|r_y(\tilde{q}_z^{-1}(q_z(i\omega)))|$ and $|r_y(i\omega)|$ in combination with Lemma 19 from Appendix A.2, we get

$$\begin{aligned} \|R(y, \tilde{V}_z)f - R(y, V)f\|_H^2 &= \int_{-iz}^{iz} |\tilde{q}_z^{-1}(q_z(i\omega)) - r_y(i\omega)|^2 d\tilde{E}_f(i\omega) \\ &= \int_{(-iz, iz) \setminus \{0\}} |\tilde{q}_z^{-1}(q_z(i\omega)) - r_y(i\omega)|^2 d\tilde{E}_f(i\omega) \\ &\leq \frac{4}{y^2} \int_{(-iz, iz) \setminus \{0\}} d\tilde{E}_f(i\omega), \end{aligned}$$

where we have used the fact that $\tilde{E}(\{0\}) = 0$ to obtain the second equality. It follows from upper continuity of finite measures that for every sequence z_1, z_2, \dots of strictly positive numbers decreasing to 0,

$$\limsup_{n \rightarrow \infty} \|R(y, \tilde{V}_{z_n})f - R(y, V)f\|_H^2 \leq \frac{4}{y^2} \tilde{E}_f\left(\bigcap_{n>0} (-iz_n, iz_n) \setminus \{0\}\right) = \frac{4}{y^2} \tilde{E}_f(\emptyset) = 0,$$

proving that $\tilde{V}_z \xrightarrow{\text{sr}} V$ on \tilde{H} . We can then conclude that $V_z \xrightarrow{\text{sr}} V$ on H by noting that $R(y, V|_{\tilde{H}}) - R(y, V_z) = (R(y, V) - R(y, \tilde{V}_z))\tilde{\Pi}$. \square

Next, let $b_z: i\mathbb{R} \rightarrow i\mathbb{R}$ be any continuous extension of \tilde{q}_z^{-1} to the entire imaginary line. For a choice of kernels $p_\tau: \mathcal{M} \times \mathcal{M} \rightarrow \mathbb{R}$ satisfying properties (K1)–(K5), we approximate Q_z by the compact operators $Q_{z,\tau}: H \rightarrow H$, $\tau > 0$, where

$$Q_{z,\tau} = R_z^* V_\tau R_z, \quad V_\tau = G_{\tau/2} V G_{\tau/2}. \quad (18)$$

Define the unbounded, skew-adjoint operator $V_{z,\tau}: D(V_{z,\tau}) \rightarrow H$ as

$$V_{z,\tau} = \tilde{V}_{z,\tau} \tilde{\Pi}, \quad \tilde{V}_{z,\tau} = b_z(Q_{z,\tau}).$$

Our main spectral approximation result is as follows.

Theorem 6. *For $z, \tau > 0$ the operators $V_{z,\tau}$ satisfy properties (P1)–(P5). As such, in the iterated limit $z \rightarrow 0^+$, $\tau \rightarrow 0^+$, $V_{z,\tau}$ converges spectrally to V in the sense of Theorem 2.*

Proof. Properties (P1)–(P4) follow from the construction of $V_{z,\tau}$. Property (P5) follows from the fact that $\lim_{\tau \rightarrow 0} G_\tau f = f$ for $f \in H$ (property (K3)), so we have $V_{z,\tau} \xrightarrow{\text{sr}} V_z$ as $\tau \rightarrow 0^+$ and the subsequent application of Theorem 5. \square

Consider now an eigendecomposition of the compact, skew-adjoint operator $Q_{z,\tau}$,

$$Q_{z,\tau} \xi_{j,z,\tau} = \beta_{j,z,\tau} \xi_{j,z,\tau}, \quad \beta_{j,z,\tau} \in i\mathbb{R}, \quad \xi_{j,z,\tau} \in \tilde{H} \setminus \{0\}, \quad (19)$$

where the eigenpairs are indexed by $j \in \mathbb{N}_0$ and $\{\xi_{j,z,\tau}\}_{j \in \mathbb{N}}$ is an orthonormal basis of \tilde{H} . Since $Q_{z,\tau}$ is a real operator (i.e., $(Q_{z,\tau} f)^* = Q_{z,\tau}(f^*)$), it follows that the eigenvectors $\xi_{j,z,\tau}$ corresponding to nonzero $\beta_{j,z,\tau}$ come in complex-conjugate pairs.

Applying b_z to the eigenvalues of $Q_{z,\tau}$ leads to an eigendecomposition of $\tilde{V}_{z,\tau}$:

$$\tilde{V}_{z,\tau} \xi_{j,z,\tau} = i\omega_{j,z,\tau} \xi_{j,z,\tau}, \quad i\omega_{j,z,\tau} = b_z(\beta_{j,z,\tau}).$$

Correspondingly, $\{\xi_{j,z,\tau}\}_{j \in \mathbb{N}} \cup \{\xi_{0,z,\tau} = \mathbf{1}\}$ is an orthonormal basis of H consisting of eigenfunctions of $\tilde{V}_{z,\tau}$ with $\xi_{0,z,\tau}$ corresponding to eigenfrequency $\omega_{0,z,\tau} = 0$.

In light of Theorem 6, we view the eigenpairs $(\omega_{j,z,\tau}, \xi_{j,z,\tau})$ as generalizations of the true generator eigenpairs (ω_j, ξ_j) from Section 2.2 that provide an orthonormal basis of H_p . Defining the unitary operators $U_{z,\tau}^t = e^{tV_{z,\tau}}$, we have

$$U_{z,\tau}^t f = \sum_{j \in \mathbb{N}_0} \langle f, \xi_{j,z,\tau} \rangle e^{i\omega_{j,z,\tau} t} \xi_{j,z,\tau}, \quad \forall f \in H, \quad (20)$$

which generalizes (4) to the entire Hilbert space H . Moreover, by equivalence of strong resolvent convergence of $V_{z,\tau}$ to V (property (P5)) and strong dynamical convergence, we have $\lim_{z \rightarrow 0^+} \lim_{\tau \rightarrow 0^+} U_{z,\tau}^t f = U^t f$, so (20) consistently approximates the true Koopman evolution of observables in H .

Remark 7. In general, the spectrum of $Q_{z,\tau}$ does not need to be a subset of the interval $i[-(2z)^{-1}, (2z)^{-1}]$ that contains the spectrum of Q_z . Still, in the numerical experiments performed in this work (see Section 5) we have not observed any cases where the inclusion $\sigma(Q_{z,\tau}) \subseteq i[-(2z)^{-1}, (2z)^{-1}]$ is violated. With such an inclusion, $b_z(\beta_{j,z,\tau}) = \tilde{q}_z^{-1}(\beta_{j,z,\tau})$ and an explicit choice of extension $b_z \supseteq \tilde{q}_z^{-1}$ is not needed.

In Section 4 below, our goal will be to produce approximations of the eigenpairs $(\omega_{j,z,\tau}, \xi_{j,z,\tau})$ using data-driven Galerkin methods for variational generalized eigenvalue problems. Besides the L^2 elements $\xi_{j,z,\tau}$, we will also be interested in smooth eigenfunctions $\zeta_{j,z,\tau}$ lying in the RKHS $\mathcal{H} \subset C^1(M)$ from Section 2.5. We obtain such eigenfunctions by applying the isometry $T: H \rightarrow \mathcal{H}$, viz.

$$\zeta_{j,z,\tau} = T \xi_{j,z,\tau}. \quad (21)$$

The resulting functions $\zeta_{j,z,\tau} \in \mathcal{H}$ are eigenvectors of the skew-adjoint operator $W_{z,\tau} := T^* V_{z,\tau} T$ on \mathcal{H} which is unitarily equivalent to $V_{z,\tau}$, and form an orthonormal basis of $\mathcal{H}(X) \subseteq \mathcal{H}$. Furthermore, from the polar decomposition (11) we get $\iota e^{tW_\tau} T = G^{1/2} e^{tV_\tau}$. From the latter and Theorem 6 we deduce that W_τ generates a smooth approximation of Koopman evolution on H (while being unitary on \mathcal{H}),

$$\lim_{\tau \rightarrow 0^+} \iota e^{tW_\tau} T f = G^{1/2} U^t f, \quad \forall f \in H.$$

4. Finite-dimensional approximation

Algorithm 1 Numerical operator approximation for training data x_0, x_1, \dots, x_{N-1} , symmetric positive-definite Markovian kernel p_N , resolvent parameter $z > 0$, smoothing parameter $\tau > 0$, and number of basis functions $L \leq N - 1$. Additionally, $\tilde{q}_z^{-1}(i\omega)$ is the function defined in (16), and \vec{V} denotes the dynamical vector field that generates the dynamics, (2). The algorithm computes a rank- L skew-adjoint operator $V_{z,\tau,L,N} \in \hat{H}_N$, along with its nonzero eigenfrequencies $\omega_{j,z,\tau,L,N}$ and eigenfunctions $\xi_{j,z,\tau,L,N}$. The corresponding operator $W_{z,\tau,L,N}$ with eigenfunctions $\hat{\zeta}_{j,z,\tau,L,N}$ in the RKHS \mathcal{H}_N is also computed.

- 1: Compute kernel eigenvectors $\{\phi_{j,N}\}_{j=0}^L$ and corresponding eigenvalues $\{\lambda_{j,N}\}_{j=0}^L$ from the kernel integral operator defined by p_N , i.e. $G_N f = \int_X p_N(\cdot, x) f(x) d\mu_N(x)$.
- 2: Define functions $\varphi_{j,N}$ to be continuous representatives of $\phi_{j,N}$ with respect to the sampling measure μ_N ; that is, $\varphi_{j,N}(x_n) = \phi_{j,N}(x_n)$ for all $n \in \{0, \dots, N-1\}$ (equivalently; $\iota_N \varphi_{j,N} = \phi_{j,N}$).
- 3: Compute eigenfunction derivatives $\{\phi'_{j,N}\}_{j=1}^L$, where $\phi'_{j,N} = \iota_N \varphi'_{j,N}$ and $\varphi'_j = \vec{V} \cdot \nabla \varphi_j$. Define the Koopman generator approximation V_N such that $V_N \phi_{j,N} = \phi'_{j,N}$.
- 4: Compute the $L \times L$ matrix representation \mathbf{V}_N of V_N with elements $\mathbf{V}_{ij,N} = \langle \phi_{i,N}, V_N \phi_{j,N} \rangle_N$. Compute $L \times L$ matrices $\mathbf{V}_N^{(2)}$ and $\tilde{\mathbf{V}}_N$, where $\mathbf{V}_{ij,N}^{(2)} = \langle V_N \phi_{i,N}, V_N \phi_{j,N} \rangle_N$, and $\tilde{\mathbf{V}}_N = (\mathbf{V}_N - \mathbf{V}_N^\top)/2$.
- 5: Define $\mathbf{A}_{\tau/2,N}$ to be the $L \times L$ matrix approximation of $G_{\tau/2}$ in the $\phi_{j,N}$ basis, where $\mathbf{A}_{\tau/2,N} = \text{diag}(\lambda_{1,\tau/2,N}, \dots, \lambda_{L,\tau/2,N})$, $\lambda_{j,\tau/2,N} = e^{-\tau \eta_{j,N}}$, and $\eta_{j,N} = \frac{\lambda_{j,N}^{-1} - 1}{\lambda_{0,N}^{-1} - 1}$.
- 6: Compute the $L \times L$ matrices $\mathbf{A}_{\tau,N} = \mathbf{A}_{\tau/2,N} \tilde{\mathbf{V}}_N \mathbf{A}_{\tau/2,N}$ and $\mathbf{B}_{z,N} = z^2 \mathbf{I} + \mathbf{V}_N^{(2)} - (\mathbf{V}_N + \mathbf{V}_N^\top)$.
- 7: Solve the matrix generalized eigenvalue problem $\mathbf{A}_{\tau,N} \mathbf{c}_j = \beta_{j,z,\tau,L,N} \mathbf{B}_{z,N} \mathbf{c}_j$ for eigenvectors \mathbf{c}_j and eigenvalues $\beta_{j,z,\tau,L,N}$.
- 8: Compute eigenfrequencies $\omega_{j,z,\tau,L} = b_z(\beta_{j,z,\tau,L})$ with corresponding eigenvectors $\xi_{j,z,\tau,L,N}$ of $V_{z,\tau,L,N}$ by $\xi_{j,z,\tau,L,N} = \sum_{i=1}^L (z \phi_{i,N} - \phi'_{i,N}) c_{ij}$. Set $\omega_{0,z,\tau,L,N} = 0$ and $\xi_{0,z,\tau,L,N}$ to be constant.
- 9: Define the functions $\varphi'_{i,L',N} := T_{L',N} \phi'_{i,N} = \sum_{j=0}^{L'-1} \langle \phi_{j,N}, \phi'_{i,N} \rangle_N \lambda_{j,N}^{1/2} \varphi_{j,N}$, where $T_{L',N}$.
- 10: Define the RKHS operator $W_{z,\tau,L,N} = \hat{T}_N^* V_{z,\tau,L,N} \hat{T}_N$ to have eigenvalues $i\omega_{j,z,\tau,L,N}$ with eigenvectors $\hat{\zeta}_{j,z,\tau,L,N}$ approximated by $\zeta_{j,z,\tau,L,L',N} := \sum_{i=1}^L (z \sigma_{i,N} \varphi_{i,N} - \varphi'_{i,L',N}) c_{ij}$.

4.1. Generalized eigenvalue problem

To take advantage of physics-informed computation of function gradients (see (1) and (10)), we transform the eigenvalue problem (19) into a generalized eigenvalue problem that replaces the resolvents in the left-hand side by a positive operator that is a quadratic polynomial of V in the right-hand side. First, for every $z \in \rho(V)$, $z - V: D(V) \rightarrow H$ is a surjective operator, so for every eigenvector $\xi_{j,z,\tau}$ there exists a unique $u_{j,z,\tau} \in D(V)$ such that $\xi_{j,z,\tau} = (z - V)u_{j,z,\tau}$, giving

$$R_z^* V_\tau u_{j,z,\tau} = \beta_{j,z,\tau} (z - V) u_{j,z,\tau}, \quad u_{j,z,\tau} \in D(V). \quad (22)$$

Next, supposing that $\beta_{j,\tau,z} \neq 0$ (which corresponds to the solutions of interest), we have $(z - V)u_{j,z,\tau} \in \text{ran } R_z^* = D(z + V)$. Thus, applying $z + V$ to the left- and right-hand sides of (22), we get

$$V_\tau u_{j,z,\tau} = \beta_{j,z,\tau} (z^2 - V^2) u_{j,z,\tau}, \quad u_{j,z,\tau} \in D(V^2), \quad \beta_{j,z,\tau} \neq 0. \quad (23)$$

Note that $z^2 - V^2$ is a strictly positive operator, i.e., $\langle f, (z^2 - V^2)f \rangle > 0$ whenever $f \neq 0$, by skew-adjointness of V .

4.2. Variational formulation

Equation (23) defines our generalized eigenvalue problem in strong form. We next transform this problem into weak (variational) form by taking the inner product of both sides by a test function $f \in D(V)$, and using skew-adjointness of V to obtain

$$\langle f, V_\tau u_{j,z,\tau} \rangle = \beta_{j,z,\tau} \langle \langle f, (z^2 - V^2) u_{j,z,\tau} \rangle \rangle = \beta_{j,z,\tau} (z^2 \langle f, u_{j,z,\tau} \rangle + \langle V f, V u_{j,z,\tau} \rangle). \quad (24)$$

To obtain a well-posed variational eigenvalue problem from (24), we introduce the Hilbert space $H_V = D(V) \cap \tilde{H}$, equipped with the inner product $\langle f, g \rangle_V := \langle f, g \rangle + \langle Vf, Vg \rangle$. Note that H_V is a Hilbert space since V is a closed operator. Moreover, H_V contains $\tilde{H}^1 := H^1 \cap \tilde{H}$ (the space of zero-mean functions in H^1) as a subspace and embeds continuously into H . Considered as an operator from H_V to H , the generator V is bounded.

By continuity and compactness of the embeddings $H_V \hookrightarrow H$ and $H \hookrightarrow H^{-1}$, respectively, H_V embeds into H^{-1} compactly, and we have:

Lemma 8. *The sesquilinear forms $A_\tau: H_V \times H_V \rightarrow \mathbb{C}$ and $B_z: H_V \times H_V \rightarrow \mathbb{C}$ with*

$$A_\tau(f, g) = \langle f, V_\tau g \rangle, \quad B_z(f, g) = z^2 \langle f, g \rangle + \langle Vf, Vg \rangle$$

satisfy the upper bounds

$$|A_\tau(f, g)| \leq C \|f\|_{H_V} \|g\|_{H^{-1}}, \quad |B_z(f, g)| \leq (1 + z^2) \|f\|_{H_V} \|g\|_{H_V}, \quad \forall f, g \in H_V \times H_V,$$

for a constant C . In addition, B_z is coercive,

$$|B_z(f, f)| \geq \min\{1, z^2\} \|f\|_{H_V}^2, \quad \forall f \in H_V.$$

Proof. Boundedness and coercivity of B_z follow from

$$\begin{aligned} |B_z(f, g)| &\leq z^2 \|f\|_H \|g\|_H + \|Vf\|_H \|Vg\|_H \\ &\leq z^2 \|f\|_{H_V} \|g\|_{H_V} + \|f\|_{H_V} \|g\|_{H_V} \\ &= (1 + z^2) \|f\|_{H_V} \|g\|_{H_V} \end{aligned}$$

and

$$\begin{aligned} |B_z(f, f)| &= z^2 (\|f\|_H^2 + z^{-2} \|Vf\|_H^2) \\ &\geq z^2 \min\{1, z^{-2}\} \|f\|_{H_V}^2 \\ &= \min\{z^2, 1\} \|f\|_{H_V}^2, \end{aligned}$$

respectively. For the upper bound on A_τ , observe that $VG_{\tau/2}$ is a bounded operator on H satisfying $\|VG_{\tau/2}\| \leq \|\vec{V} \cdot \nabla\| \|p_{\tau/2}\|_{C^1(M \times M)}$, where the operator norm $\|\vec{V} \cdot \nabla\|$ is taken on $B(C^1(M), C(M))$. Using this fact and boundedness of $G^{-1}G_\tau$ (see Section 2.4), we compute

$$\begin{aligned} |A_\tau(f, g)| &= |\langle VG_{\tau/2}f, G_{\tau/2}g \rangle| \\ &\leq \|VG_{\tau/2}f\|_H \|G_{\tau/2}g\|_H \\ &\leq \|VG_{\tau/2}\| \|f\|_H \|G_{\tau/2}G^{-1}\| \|Gg\|_H \\ &= \|VG_{\tau/2}\| \|G_{\tau/2}G^{-1}\| \|f\|_H \|g\|_{H^{-1}} \\ &\leq \|VG_{\tau/2}\| \|G_{\tau/2}G^{-1}\| \|f\|_{H_V} \|g\|_{H^{-1}}. \end{aligned}$$

which implies the claimed upper bound for $C = \|VG_{\tau/2}\| \|G_{\tau/2}G^{-1}\|$. \square

Results on variational eigenvalue problems [e.g., 32, section 8], Lemma 8, and compactness of the embedding $H_V \hookrightarrow H^{-1}$ imply the existence of a compact operator $T_{z,\tau}: H_V \rightarrow H_V$ such that $\alpha A_\tau(f, u) = B_z(f, u)$ holds for some $u \neq 0$ for all $f \in H_V$ if and only if $\alpha T_{z,\tau}u = u$; i.e., (α^{-1}, u) is an eigenpair of $T_{z,\tau}$ whenever $\alpha \neq 0$. Putting together these facts, we deduce that the following is a well-posed variational eigenvalue problem, yielding solutions of (23) in H_V .

Definition 9 (variational eigenvalue problem for $Q_{z,\tau}$). Find $\beta_{j,z,\tau} \in \mathbb{C}$ and $u_{j,z,\tau} \in H_V \setminus \{0\}$ such that

$$A_\tau(f, u_{j,z,\tau}) = \beta_{j,z,\tau} B_z(f, u_{j,z,\tau}), \quad \forall f \in H_V.$$

For every solution $(\beta_{j,z,\tau}, u_{j,z,\tau})$ of this problem with $\beta_{j,z,\tau} \neq 0$ we have that

$$\xi_{j,z,\tau} = (z - V)u_{j,z,\tau} \quad (25)$$

is an eigenvector of $Q_{z,\tau}$ with corresponding eigenvalue $\beta_{j,z,\tau}$. Conversely, for every eigenvector $\xi_{j,z,\tau}$ of $Q_{z,\tau}$ corresponding to nonzero eigenvalue $\beta_{j,z,\tau}$, $(\beta_{j,z,\tau}, u_{j,z,\tau})$ with $u_{j,z,\tau} = R_z \xi_{j,z,\tau}$ solves the problem in Definition 9. Furthermore, since $u_{j,z,\tau}$ lies in $\text{ran } G_{\tau/2} \subset H^1$, it has a representative in $\tilde{u}_{j,z,\tau} \in \mathcal{H} \subset C^1(M)$ obtained via the Nystrom operator from (14) as $\tilde{u}_{j,z,\tau} = \mathcal{N}u_{j,z,\tau}$. As a result, $\xi_{j,z,\tau}$ has a continuous representative

$$\tilde{\xi}_{j,z,\tau} = (z - \vec{V} \cdot \nabla) \tilde{u}_{j,z,\tau} \in C(M), \quad \iota \tilde{\xi}_{j,z,\tau} = \xi_{j,z,\tau}.$$

We obtain the corresponding smooth eigenfunctions $\zeta_{j,z,\tau} \in \mathcal{H}$ of $W_{z,\tau}$ via (21).

4.3. Galerkin scheme

We compute approximate solutions of the variational eigenvalue problem in Definition 9 using Galerkin methods. To that end, we first establish that the kernel eigenfunctions ϕ_j from Section 2.4 provide a dense subspace $\tilde{E} := \text{span}\{\phi_1, \phi_2, \dots\}$ of H_V , in which we will compute approximate solutions. Defining $E = \text{span}\{\phi_0, \phi_1, \dots\}$ and using (\cdot) to denote operator closure, the density of \tilde{E} in H_V will be a corollary of the following proposition.

Proposition 10. *The restriction $V|_E$ of V onto E is a well-defined, essentially skew-adjoint operator; that is, $\overline{V|_E} = V$.*

Proof. Well-definition of $V|_E$ follows from the fact that ϕ_j lies in $D(V)$ for all $j \in \mathbb{N}_0$ (see Section 2.4). For essential skew-adjointness, recall that a necessary and sufficient condition for a symmetric operator $A: D(A) \rightarrow H$ to be essentially self-adjoint is that the images $(i \pm A)(D(A))$ are dense in H [e.g., 33, Section VIII.2]. Letting $A = (V|_E)/i$, it follows that $V|_E$ is essentially skew-adjoint iff $(1 \pm V)E$ are dense subspaces of H . Suppose that f is an element of $D(V)$ such that $f \in ((1 - V)E)^\perp$. Then for all $j \in \mathbb{N}_0$, we have that $\langle (1 - V)\phi_j, f \rangle = 0$, so $\langle \phi_j, (1 + V)f \rangle = 0$. Since $\{\phi_j\}_{j \in \mathbb{N}_0}$ is an orthonormal basis of H , we have $(1 + V)f = 0$ which implies that $f = 0$ because V has no eigenvalues equal to -1 . This implies that $((1 - V)E)^\perp \subseteq D(V)^\perp = \{0\}$. We can then conclude that $(1 - V)E$ is dense in H . A similar argument shows that $(1 + V)E$ is also dense in H . The proposition then follows. \square

Corollary 11. *The space \tilde{E} is a dense subspace of H_V .*

Proof. Let $G(A) = \{(f, Af) \in H \times H : f \in D(A)\}$ denote the graph of an operator $A: D(A) \rightarrow H$. The graph $G(A)$ is equipped with the inner product $\langle (f, Af), (g, Ag) \rangle_{G(A)} = \langle f, g \rangle + \langle Af, Ag \rangle$, and it is canonically isomorphic to $D(A)$ equipped with the inner product $\langle f, g \rangle_A = \langle f, g \rangle + \langle Af, Ag \rangle$. Explicitly, the isomorphism $\epsilon_A: D(A) \rightarrow G(A)$ is given by $\epsilon_A f = (f, Af)$. Since $V = \overline{V|_E}$, we have that $G(V) = \overline{G(V|_E)}^{\|\cdot\|_{H \times H}}$. We also have that $G(V) = \epsilon_V(D(V))$ and $G(V|_E) = \epsilon_{V|_E}(E) = \epsilon_V E$. As such, we get $\epsilon_V(H_V) = \overline{\epsilon_V(E)}^{\|\cdot\|_{H \times H}}$, which implies $D(V) = \overline{E}^{\|\cdot\|_{D(V)}}$. Since $H_V = \tilde{\Pi}(D(V))$ and $\tilde{E} = \tilde{\Pi}E$, it follows that $H_V = \overline{\tilde{E}}^{\|\cdot\|_{H_V}}$, proving the corollary. \square

For $L \in \mathbb{N}$, consider the approximation spaces $E_L = \text{span}\{\phi_1, \dots, \phi_L\}$ and the orthogonal projections $\Pi_L: H \rightarrow H$ and $\Pi_{V,L}: H_V \rightarrow H_V$ with $\text{ran } \Pi_L = E_L \subset H$ and $\text{ran } \Pi_{V,L} = E_L \subset H_V$. Note that $\Pi_{V,L}$ converges strongly to the identity on H_V as $L \rightarrow \infty$ by Corollary 11. Our Galerkin method solves the following problem.

Definition 12 (variational eigenvalue problem for $Q_{z,\tau}$; Galerkin approximation). Find $\beta_{j,z,\tau,L} \in \mathbb{C}$ and $u_{j,z,\tau,L} \in E_L \setminus \{0\}$ such that

$$A_z(f, u_{j,z,\tau,L}) = \beta_{j,z,\tau,L} B_z(f, u_{j,z,\tau,L}), \quad \forall f \in E_L.$$

For every solution $(\beta_{j,z,\tau,L}, u_{j,z,\tau,L})$ we define $\xi_{j,z,\tau,L} \in H$ as

$$\xi_{j,z,\tau,L} = (z - V)u_{j,z,\tau,L},$$

the continuous representative $\tilde{\xi}_{j,z,\tau,L} \in C(M)$ as

$$\tilde{\xi}_{j,z,\tau,L} = (z - \vec{V} \cdot \nabla) \tilde{u}_{j,z,\tau,L}, \quad \tilde{u}_{j,z,\tau,L} = \mathcal{N}u_{j,z,\tau,L}, \quad (26)$$

and the RKHS function $\zeta_{j,z,\tau,L} \in \mathcal{H}$ as

$$\zeta_{j,z,\tau,L} = T\xi_{j,z,\tau,L},$$

where $\iota\tilde{\xi}_{j,z,\tau,L} = \xi_{j,z,\tau,L}$. One can directly verify that any two eigenvectors $\xi_{j,z,\tau,L}$ (resp. $\zeta_{j,z,\tau,L}$) corresponding to distinct eigenvalues $\beta_{j,z,\tau,L}$ are orthogonal in H (resp. \mathcal{H}), and any linearly independent set corresponding to the same eigenvalue can be chosen to be orthogonal. Moreover, when L is even, the eigenvalues/eigenvectors come in complex-conjugate pairs, similarly to the eigenvalues/eigenvectors of the infinite-rank operator $Q_{z,\tau}$. Henceforth, we shall assume that L is chosen even.

We have $\lim_{L \rightarrow \infty} \|\Pi_{V,L}f - f\|_{H_V} = 0$ for all $f \in H_V$ by Corollary 11. Moreover, by boundedness and coercivity of B_z on $H_V \times H_V$ (Lemma 8), for every $f \in H_V \setminus \{0\}$ there exists $L_* \in \mathbb{N}$ and $c > 0$ such that $B_z(f, f) \geq c$ holds for all $L > L_*$. By results on Galerkin approximation of variational eigenvalue problems [e.g., 32] these facts imply that, as $L \rightarrow \infty$, every nonzero $\beta_{j,z,\tau,L}$ converges to $\beta_{j,z,\tau}$ and that the corresponding eigenspaces — $\mathbb{E}_{j,z,\tau}^{(V)} := \text{span}\{u_{i,z,\tau} : \beta_{i,z,\tau} = \beta_{j,z,\tau}\}$ and $\mathbb{E}_{j,z,\tau,L}^{(V)} := \text{span}\{u_{i,z,\tau,L} : \beta_{i,z,\tau,L} = \beta_{j,z,\tau,L}\}$ — converge in the sense of strong convergence of orthogonal projections. That is, with $\mathcal{U}_{j,z,\tau} : H_V \rightarrow H_V$ and $\mathcal{U}_{j,z,\tau,L} : H_V \rightarrow H_V$ denoting the orthogonal projections onto $\mathbb{E}_{j,z,\tau}^{(V)}$ and $\mathbb{E}_{j,z,\tau,L}^{(V)}$, we have

$$\lim_{L \rightarrow \infty} \|\mathcal{U}_{j,z,\tau,L}f - \mathcal{U}_{j,z,\tau}f\|_{H_V} = 0, \quad \forall f \in H_V.$$

Since V is bounded as linear map from H_V to H , it follows additionally that $\lim_{L \rightarrow \infty} \|(z - V)(\mathcal{U}_{j,z,\tau,L} - \mathcal{U}_{j,z,\tau})f\|_H = 0$ for every $f \in H_V$. This implies in turn that the orthogonal projections $\Xi_{j,z,\tau,L} : H \rightarrow H$ onto the subspaces $\mathbb{E}_{j,z,\tau,L} := \text{span}\{\xi_{i,z,\tau,L} : \beta_{i,z,\tau,L} = \beta_{j,z,\tau,L}\} \subset H$ converge strongly to the orthogonal projections $\Xi_{j,z,\tau} : H \rightarrow H$ onto $\mathbb{E}_{j,z,\tau} := \text{span}\{\xi_{i,z,\tau} : \beta_{i,z,\tau} = \beta_{j,z,\tau}\} \subset H$, i.e.,

$$\lim_{L \rightarrow \infty} \|\Xi_{j,z,\tau}f - \Xi_{j,z,\tau,L}f\|_H = 0, \quad \forall f \in H.$$

Defining the frequencies $\omega_{j,z,\tau,L} = b_z(\beta_{j,z,\tau,L})/i$ and the skew-adjoint, finite-rank operators $Q_{z,\tau,L} : \tilde{H} \rightarrow \tilde{H}$, $\tilde{V}_{z,\tau,L} = b_z(Q_{z,\tau,L})$, and $V_{z,\tau,L} : H \rightarrow H$, where

$$Q_{z,\tau,L} = \sum_{j=1}^L \beta_{j,z,\tau,L} \xi_{j,z,\tau,L} \langle \xi_{j,z,\tau,L}, \cdot \rangle, \quad \tilde{V}_{z,\tau,L} = \sum_{j=1}^L i\omega_{j,z,\tau,L} \xi_{j,z,\tau,L} \langle \xi_{j,z,\tau,L}, \cdot \rangle,$$

and $V_{z,\tau,L} = \tilde{\Pi} \tilde{V}_{z,\tau,L} \tilde{\Pi}$, we have the following proposition:

Proposition 13. *As $L \rightarrow \infty$, $Q_{z,\tau,L}$ converges to $Q_{z,\tau}$ strongly, and $V_{z,\tau,L}$ converges to $V_{z,\tau}$ in strong resolvent sense.*

Proof. The strong convergence of $Q_{z,\tau,L}$ to $Q_{z,\tau}$ is a direct consequence of the spectral convergence $\beta_{j,z,\tau,L} \rightarrow \beta_{j,\tau}$ and $\Xi_{j,z,\tau,L} \xrightarrow{s} \Xi_{j,z,\tau}$. Next, observe that, for $z > 0$, the resolvent function $r_z : i\mathbb{R} \rightarrow \mathbb{C}$, $r_z(i\omega) = z - (i\omega)^{-1}$ is a bounded continuous function that maps the imaginary line to the circle in the complex plane with radius $(2z)^{-1}$ and center $(2z)^{-1}$ [see, e.g., 21]. Since $\tilde{R}_{z,\tau} = r_z \circ b_z(Q_z)$ and $\tilde{R}_{z,\tau,L} = r_z \circ b_z(Q_{z,\tau,L})$ give the resolvents of $\tilde{V}_{z,\tau}$ and $\tilde{V}_{z,\tau,L}$, respectively, the strong convergence $\tilde{R}_{z,\tau,L} \xrightarrow{s} \tilde{R}_{z,\tau}$ follows from strong convergence of $Q_{z,\tau,L}$ to $Q_{z,\tau}$ and boundedness and continuity of $r_z \circ b_z$. The strong convergence of the resolvent $R_{z,\tau,L}$ of $V_{z,\tau,L}$ to $R_{z,\tau}$ follows from $R_{z,\tau,L} \xrightarrow{s} R_{z,\tau}$ and the facts that $R_{z,\tau,L} = \tilde{R}_{z,\tau,L} + z^{-1}\Pi_0$ and $R_{z,\tau} = \tilde{R}_{z,\tau} + z^{-1}\Pi_0$. \square

Similarly to the infinite-rank operator $V_{z,\tau}$, $V_{z,\tau,L}$ is unitarily equivalent to a skew-adjoint operator $W_{z,\tau,L} = T^*V_{z,\tau,L}T$ acting on the RKHS \mathcal{H} , where

$$W_{z,\tau,L} = \sum_{j=1}^L i\omega_{j,z,\tau,L} \zeta_{j,z,\tau,L} \langle \zeta_{j,z,\tau,L}, \cdot \rangle_{\mathcal{H}}.$$

This operator has eigenvectors $\zeta_{j,z,\tau,L} \in \mathcal{H}$, and can be thought of as generating a smooth approximation of the evolution in H generated by $V_{z,\tau,L}$; see Section 3.

Next, to examine the above Galerkin approximation from a computational standpoint, define the $L \times L$ generator matrix $\mathbf{V} = [V_{ij}]_{i,j=1}^L$ with entries $V_{ij} = \langle \phi_i, V\phi_j \rangle = -V_{ji}$. Note that for the kernel construction described in Section 2.4, we can use (10) to express V_{ij} using the singular vectors of the integral operator \tilde{K} and the directional derivative kernel \hat{k}' , i.e.,

$$V_{ij} = \langle \phi_i, \tilde{K}'\gamma_j \rangle \equiv \int_X \int_X \phi_i(x) (\vec{V}_x \cdot \hat{k}(x, z)) \gamma_j(z) d\mu(x) d\mu(z). \quad (27)$$

In particular, under our assumption of known dynamical vector field \vec{V} , the integrand in the right-hand side can be evaluated in a physics-informed manner by computing derivatives of the kernel function \hat{k} . In the experiments of Section 5, we perform these computations using automatic differentiation. Defining $\mathbf{V}^{(2)} = [V_{ij}^{(2)}]_{i,j=1}^L$ as the $L \times L$ symmetric positive-definite matrix with elements $V_{ij}^{(2)} = \langle V\phi_i, V\phi_j \rangle$, we have

$$V_{ij}^{(2)} = \langle \tilde{K}'\gamma_i, \tilde{K}'\gamma_j \rangle \equiv \int_X \int_X \int_X \gamma_i(y) (\vec{V}_x \cdot \hat{k}(x, y)) (\vec{V}_x \cdot \hat{k}(x, z)) \gamma_j(z) d\mu(x) d\mu(y) d\mu(z). \quad (28)$$

In what follows, $\mathbf{\Lambda}_\tau$ will be the $L \times L$ diagonal matrix equal to $\text{diag}(\lambda_{1,\tau}, \dots, \lambda_{L,\tau})$, and \mathbf{I} will be the $L \times L$ identity matrix.

Expanding $u_{j,z,\tau,L} = \sum_{i=1}^L c_{ij}\phi_i$, $c_{ij} \in \mathbb{C}$, and forming the column vector $\mathbf{c}_j = (c_{1j}, \dots, c_{Lj})^\top \in \mathbb{C}^L$ of expansion coefficients, solutions of the variational problem in Definition 12 can be equivalently obtained by solving the matrix generalized eigenvalue problem

$$\mathbf{A}_\tau \mathbf{c}_j = \beta_{j,z,\tau,L} \mathbf{B}_z \mathbf{c}_j, \quad (29)$$

where $\mathbf{A}_\tau := [A_\tau(\phi_i, \phi_j)]_{i,j=1}^L$ and $\mathbf{B}_z := [B_z(\phi_i, \phi_j)]_{i,j=1}^L$ are $L \times L$ matrix representations of the sesquilinear forms A_τ and B_z , respectively, on E_L . Explicitly, we have

$$\mathbf{A}_\tau = \mathbf{\Lambda}_{\tau/2} \mathbf{V} \mathbf{\Lambda}_{\tau/2}, \quad \mathbf{B}_z = z^2 \mathbf{I} + \mathbf{V}^{(2)}$$

Moreover, the corresponding eigenvectors $\xi_{j,z,\tau,L}$ and $\zeta_{j,z,\tau,L}$ of $V_{z,\tau,L}$ and $W_{z,\tau,L}$, respectively, can be obtained from

$$\xi_{j,z,\tau,L} = \sum_{i=1}^L (z\phi_i - \phi'_i) c_{ij}, \quad \zeta_{j,z,\tau,L} = \sum_{i=1}^L (z\sigma_i \phi_i - T\phi'_i) c_{ij}, \quad (30)$$

where the directional derivatives $\phi'_i \in H$ are computed again via automatic differentiation using (10) and the RKHS functions $T\phi'_i$ are given by (12). Note that, in general, computation of $T\phi'_i$ via (12) requires evaluation of an infinite linear combination of RKHS basis functions ψ_i . In practical applications, we can use the partial isometries $T_{L'}$ from (13) to truncate this sum to a finite number of terms $L' \in \mathbb{N}$. This leads to the approximation

$$\zeta_{j,z,\tau,L,L'} := \sum_{i=1}^L (z\sigma_i \phi_i - \phi'_{i,L'}) c_{ij}, \quad \phi'_{i,L'} := T_{L'} \phi'_i, \quad (31)$$

which converges to $\zeta_{j,z,\tau,L}$ as $L' \rightarrow \infty$ in the norm of \mathcal{H} . For completeness, we note the formula $\tilde{\xi}_{j,z,\tau,L} = \sum_{i=1}^L (z\phi_i - \phi'_i) c_{ij} \in C(M)$ for the continuous representative $\tilde{\xi}_{j,z,\tau,L}$ of $\xi_{j,z,\tau,L}$ from (26).

4.4. Data-driven approximation

Practical implementation of the Galerkin scheme described in Section 4.3 relies on evaluation of the integrals for the generator matrix elements V_{ij} in (27). Even if the dynamical vector field \vec{V} is known, these integrals cannot typically be evaluated in closed form, e.g., due to lack of explicit knowledge of the kernel eigenbasis and/or the invariant measure. As a result, one must oftentimes resort to numerical approximation of these integrals. Our main focus is on data-driven quadrature schemes, where integrals with respect to the invariant measure μ are approximated by ergodic time averaging along numerical trajectories.

Let x_0, x_1, \dots be a sequence of points in M that is equidistributed with respect to μ . This means that the sampling measures $\mu_N := \sum_{n=0}^{N-1} \delta_{x_n}/N$ converge to the invariant measure in the sense of weak-* convergence of Borel measures on the compact manifold M ,

$$\lim_{N \rightarrow \infty} \int_M f d\mu_N = \int_M f d\mu, \quad \forall f \in C(M). \quad (32)$$

Under the ergodicity assumption in Section 2.1, μ -a.e. initial condition x_0 and Lebesgue-a.e. sampling interval $\Delta t > 0$ will yield a sequence $x_n = \Phi^{n\Delta t}(x_0)$ satisfying (32). Moreover, for systems with so-called observable ergodic invariant measures [e.g., 34], x_0 may be drawn from a subset of M of positive ambient measure (e.g., volume measure induced from a Riemannian metric). While little can be said about rates of convergence of $\int_M f d\mu_N$ to $\int_M f d\mu$ for arbitrary dynamical systems and observables, there are examples (oftentimes involving hyperbolic dynamics) exhibiting central limit theorems for sufficiently smooth observables [1], with corresponding $O(N^{-1/2})$ rates. An analysis of convergence rates is beyond the scope of this paper. However, it is worthwhile noting that the fact that our scheme does not require time-ordered snapshots (by virtue of using known equations of motion) provides flexibility in the strategy employed to generate the samples x_n . For example, grid-based quadrature or Markov chain Monte Carlo would also be suitable, so long as the matrices involved in the variational eigenvalue problem in Definition 12 can be consistently approximated as $N \rightarrow \infty$.

For a given sampling measure μ_N , our data-driven approximation scheme is built by replacing the infinite-dimensional Hilbert space $H = L^2(\mu)$ by the finite-dimensional space $\hat{H}_N := L^2(\mu_N)$ with inner product $\langle f, g \rangle_N := \int_M f^* g d\mu_N \equiv \sum_{j=0}^{N-1} f^*(x_n)g(x_n)/N$. For simplicity of exposition, we will tacitly assume that the points x_n are all distinct so that \hat{H}_N has dimension N . The finite set $X_N = \{x_0, \dots, x_{N-1}\} \subset M$ will then denote the support of μ_N .

We construct data-driven versions of the kernel $p: M \times M \rightarrow \mathbb{R}_+$, the integral operator $G: H \rightarrow H$, the SVD ($\phi_j \in H, \sigma_j \in \mathbb{R}_+, \gamma_j \in H$) of the kernel integral operator $\hat{K}: H \rightarrow H$, the eigenvalues $\lambda_j, \lambda_{j,\tau}$, and the continuously differentiable representatives $\varphi_j \in C^1(M)$ of ϕ_j analogously to the procedure described in Section 2.4, replacing throughout the invariant measure μ by μ_N , and the initial kernel k is chosen to have variable bandwidth (see Appendix B). The resulting data-driven objects will be denoted using N subscripts, with additional $\hat{(\cdot)}$ accents when needed to avoid confusion with symbols already introduced in previous sections, e.g., $p_N: M \times M \rightarrow \mathbb{R}$, $\hat{G}_N: \hat{H}_N \rightarrow \hat{H}_N$, $\phi_{j,N} \in \hat{H}_N$, $\sigma_{j,N} \in \mathbb{R}_+$, $\gamma_{j,N} \in \hat{H}_N$, $\lambda_{j,N}, \lambda_{j,\tau,N} \in \mathbb{R}_+$, and $\varphi_{j,N} \in C^1(M)$. Moreover, $\iota_N: C(M) \rightarrow \hat{H}_N$ will denote the restriction map from continuous functions on M to equivalence classes of discretely sampled functions in \hat{H}_N . Note that the functions $\varphi_{j,N}$ are continuous representatives of $\phi_{j,N}$ with respect to the sampling measure μ_N . That is, we have $\varphi_{j,N}(x_n) = \phi_{j,N}(x_n)$ for all $n \in \{1, \dots, N-1\}$ (equivalently, $\iota_N \varphi_{j,N} = \phi_{j,N}$).

Further discussion of these constructions along with convergence results in the large-data limit, $N \rightarrow \infty$, can be found in DGV. In brief, using results on spectral approximation of kernel integral operators [e.g., 35], it can be shown that every (strictly positive) eigenvalue λ_j of G can be approximated by eigenvalues of \hat{G}_N ,

$$\lim_{N \rightarrow \infty} \lambda_{j,N} = \lambda_j, \quad (33)$$

and for every corresponding eigenfunction $\phi_j \in H$ with continuous representative φ_j there exists a sequence of eigenfunctions $\phi_{j,N} \in \hat{H}_N$ whose continuous representatives $\varphi_{j,N}$ converge to φ_j in $C(M)$ norm.

In what follows, $\mathcal{H}_N \subset C^1(M)$ will be the RKHS with reproducing kernel p_N , and $\hat{T}_N: \hat{H}_N \rightarrow \mathcal{H}_N$, $\mathcal{N}_N: \hat{H}_N \rightarrow \mathcal{H}_N$, and $\mathcal{E}_N: \hat{H}_N \rightarrow \mathbb{R}_+$ the corresponding isometric embedding, Nyström operator and

Dirichlet energy, respectively. Note that \mathcal{N}_N and \mathcal{E}_N are defined on the entire Hilbert space \hat{H}_N by finite dimensionality of this space (unlike their densely defined counterparts \mathcal{N} and \mathcal{E} , respectively, on the infinite-dimensional Hilbert space H). We also let $\psi_{j,N}$ be orthonormal basis vectors of $\mathcal{H}_N(X_N)$, defined analogously to ψ_j in the case of $\mathcal{H}(X)$. For the purposes of the physics-informed scheme studied in this paper (which requires evaluation of directional derivatives $\vec{V} \cdot \nabla$ along the dynamical vector field), we augment properties (K1)–(K5) required of the kernels p_τ by an additional assumption on C^1 -norm convergence of eigenfunctions.

(K6) For every $j \in \mathbb{N}_0$ (and sufficiently large N) the eigenfunctions $\phi_{j,N} \in \hat{H}_N$ of $G_{\tau,N}$ are chosen such that their corresponding representatives $\varphi_{j,N} \in C^1(M)$ have a $C^1(M)$ limit φ_j ,

$$\lim_{N \rightarrow \infty} \|\varphi_{j,N} - \varphi_j\|_{C^1(M)} = 0,$$

where φ_j is the $C^1(M)$ representative of the eigenfunction $\phi_j \in H$ from (9).

We then have:

Proposition 14. *For the kernel construction described in Section 2.4, every eigenfunction ϕ_j of G_τ has a corresponding sequence of eigenfunctions $\phi_{j,N}$ of $G_{\tau,N}$ satisfying property (K6).*

Proof. See Appendix A.1. □

Remark 15. The reason that property (K6) requires a choice of eigenfunctions $\varphi_{j,N}$ is that eigenvectors of linear operators are arbitrary up to multiplication by nonzero scalars, or up to a general invertible linear combination for multidimensional eigenspaces. An equivalent way of formulating the assumption without invoking a choice of eigenfunctions (but at the expense of introducing new notation) would be to require strong convergence of spectral projections onto the corresponding eigenspaces.

With these assumptions and results in place, we consider the following approximation $\hat{V}_N: \hat{H}_N \rightarrow C(M)$ of the dynamical vector field $\vec{V} \cdot \nabla: C^1(M) \rightarrow C(M)$,

$$\hat{V}_N = (\vec{V} \cdot \nabla) \circ \mathcal{N}_N,$$

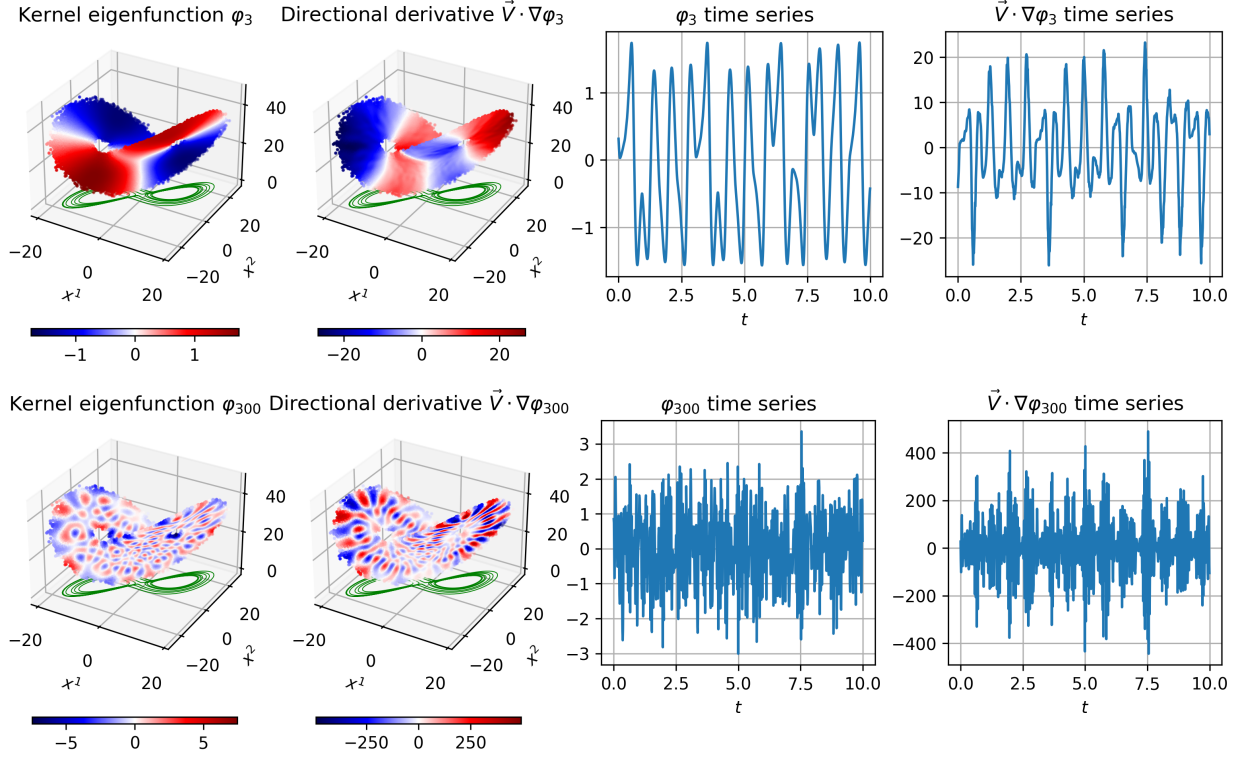
and the approximation $V_N: \hat{H}_N \rightarrow \hat{H}_N$ of the generator V given by $V_N = \iota_N \circ \hat{V}_N$. Unlike the true generator V , V_N is in general not antisymmetric, so we also employ an antisymmetric approximation, $\tilde{V}_N = (V_N - V_N^*)/2$, where the adjoint is taken on \hat{H}_N . Figure 2 shows plots of the $C^1(M)$ representative $\varphi_{j,N} = \mathcal{N}_N \phi_{j,N}$ and the directional derivative $\varphi'_{j,N} = \vec{V} \cdot \nabla \varphi_{j,N} \equiv \hat{V}_N \phi_{j,N}$ for a kernel eigenfunction $\phi_{j,N}$ computed from a dataset sampled near the Lorenz attractor in \mathbb{R}^3 (to be used in the numerical experiments of Section 5).

Next, as a data-driven analog of the space H_V from Section 4.3, we use $H_{V,N}$ — this space is equal to \hat{H}_N as a vector space but equipped with the inner product $\langle f, g \rangle_{V_N} := \langle f, g \rangle_N + \langle V_N f, V_N g \rangle_N$. Moreover, as analogs of the subspaces \tilde{E} and E_1, E_2, \dots , respectively, we define $\tilde{E}_N = \text{span}\{\phi_{1,N}, \dots, \phi_{N-1,N}\}$ and $E_{L,N} = \text{span}\{\phi_{1,N}, \dots, \phi_{L,N}\}$ for $L \in \{1, \dots, N\}$. Note that since $\phi_{0,N}$ can be chosen as the constant vector $\mathbf{1}_N := \iota_N \mathbf{1}$ (by Markovianity of \hat{G}_N), we have that \tilde{E}_N is equal as a vector space to $\tilde{H}_N := \{f \in \hat{H}_N : \langle \mathbf{1}_N, f \rangle_N = 0\}$; i.e., the space of zero-mean functions with respect to the sampling measure μ_N . In what follows, $\tilde{\Pi}_N$ and $\Pi_{L,N}$ will be the orthogonal projections on \hat{H}_N mapping into \tilde{H}_N and $E_{L,N}$ respectively.

Using the approximate generator V_N and its antisymmetric version \tilde{V}_N , we define sesquilinear forms $A_{\tau,N}: H_{V,N} \times H_{V,N} \rightarrow \mathbb{C}$ and $B_{z,N}: H_{V,N} \times H_{V,N} \rightarrow \mathbb{C}$ that will serve as data-driven analogs of A_τ and B_z from Lemma 8,

$$A_{\tau,N}(f, g) = \langle f, V_{\tau,N} g \rangle_N, \quad B_{z,N}(f, g) = z^2 \langle (z - V_N) f, (z - V_N) g \rangle_N,$$

where $V_{\tau,N} = G_{\tau/2,N} \tilde{V}_N G_{\tau/2,N}$. With these definitions, the data-driven version of the Galerkin-approximated variational eigenvalue problem from Definition 12 is as follows.



Definition 16 (variational eigenvalue problem for $Q_{z,\tau}$; data-driven approximation). Find $\beta_{j,z,\tau,L,N} \in \mathbb{C}$ and $u_{j,z,\tau,L,N} \in E_{L,N} \setminus \{0\}$ such that

$$A_{\tau,N}(f, u_{j,z,\tau,L,N}) = \beta_{j,z,\tau,L,N} B_{z,N}(f, u_{j,z,\tau,L,N}), \quad \forall f \in E_{L,N}.$$

Similarly to Section 4.3, for every solution $(\beta_{j,z,\tau,L,N}, u_{j,z,\tau,L,N})$ we compute $\xi_{j,z,\tau,L,N} = (z - V_N)u_{j,z,\tau,L,N} \in E_{L,N}$, the continuous representative $\tilde{\xi}_{j,z,\tau,L,N} = \mathcal{N}_N \xi_{j,z,\tau,L,N} \in C(M)$, the RKHS eigenfunction $\hat{\xi}_{j,z,\tau,L,N} = \hat{T}_N \xi_{j,z,\tau,L,N} \in \mathcal{H}_N$, and the corresponding eigenfrequency $\omega_{j,z,\tau,L,N} = b_z(\beta_{j,z,\tau,L,N})/i \in \mathbb{R}$. The vectors $\xi_{j,z,\tau,L,N}$ can again be chosen to form an orthonormal basis of $E_{L,N}$ with respect to the $\langle \cdot, \cdot \rangle_N$ inner product. Together with the corresponding eigenvalues and eigenfrequencies, they reconstruct skew-adjoint operators $Q_{z,\tau,L,N}: \tilde{H}_N \rightarrow \tilde{H}_N$, $\tilde{V}_{z,\tau,L,N} = b_z(Q_{z,\tau,L,N})$, and $V_{z,\tau,L,N}: \hat{H}_N \rightarrow \hat{H}_N$, where

$$\begin{aligned} Q_{z,\tau,L,N} &= \sum_{j=1}^L \beta_{j,z,\tau,L,N} \xi_{j,z,\tau,L,N} \langle \xi_{j,z,\tau,L,N}, \cdot \rangle_N, \\ \tilde{V}_{z,\tau,L,N} &= \sum_{j=1}^L i \omega_{j,z,\tau,L,N} \xi_{j,z,\tau,L,N} \langle \xi_{j,z,\tau,L,N}, \cdot \rangle_N, \\ V_{z,\tau,L,N} &= \tilde{\Pi}_N \tilde{V}_{z,\tau,L,N} \tilde{\Pi}_N. \end{aligned}$$

Moreover, $V_{z,\tau,L,N}$ is unitarily equivalent to a skew-adjoint operator $W_{z,\tau,L,N} = T_N^* V_{z,\tau,L,N} T_N$ acting on the RKHS \mathcal{H}_N , where

$$W_{z,\tau,L,N} = \sum_{j=1}^L i \omega_{j,z,\tau,L,N} \zeta_{j,z,\tau,L,N} \langle \zeta_{j,z,\tau,L,N}, \cdot \rangle_{\mathcal{H}_N}.$$

Computationally, solving the variational eigenvalue problem in Definition 16 is equivalent to solving the generalized eigenvalue problem

$$\mathbf{A}_{\tau,N} \mathbf{c}_j = \beta_{j,z,\tau,L,N} \mathbf{B}_{z,N} \mathbf{c}_j, \quad (34)$$

where $\mathbf{A}_{\tau,N} := [A_{\tau,N}(\phi_{i,N}, \phi_{j,N})]_{i,j=1}^L$ and $\mathbf{B}_{z,N} := [B_{z,N}(\phi_{i,N}, \phi_{j,N})]_{i,j=1}^L$ are $L \times L$ matrices representing $A_{\tau,N}$ and $B_{z,N}$, respectively, and $\mathbf{c}_j = (c_{1j}, \dots, c_{Lj})^\top \in \mathbb{C}^L$ is a column vector containing the expansion coefficients c_{ij} of $u_{j,z,\tau,L,N}$ in the $\phi_{i,N}$ basis of $E_{L,N}$. Aside from differences owing to non-antisymmetry of V_N , the matrices $\mathbf{A}_{\tau,N}$ and $\mathbf{B}_{z,N}$ can be computed similarly to \mathbf{A}_τ and \mathbf{B}_z , respectively, in the eigenvalue problem (34). Specifically, we have

$$\mathbf{A}_{\tau,N} = \mathbf{\Lambda}_{\tau/2,N} \tilde{\mathbf{V}}_N \mathbf{\Lambda}_{\tau/2,N}, \quad \mathbf{B}_{z,N} = z^2 \mathbf{I} + \mathbf{V}_N^{(2)} - (\mathbf{V}_N + \mathbf{V}_N^\top),$$

where $\mathbf{\Lambda}_{\tau/2,N} = \text{diag}(\lambda_{1,\tau/2,N}, \dots, \lambda_{L,\tau/2,N})$, $\tilde{\mathbf{V}}_N = (\mathbf{V}_N - \mathbf{V}_N^\top)/2$, $\mathbf{V}_N = [V_{ij,N}]_{i,j=1}^L$, and $\mathbf{V}_N^{(2)} = [V_{ij,N}^{(2)}]_{i,j=1}^L$ with $V_{ij,N} = \langle \phi_{i,N}, V_N \phi_{j,N} \rangle_N$ and $V_{ij,N}^{(2)} = \langle V_N \phi_{i,N}, V_N \phi_{j,N} \rangle_N$. Figure 3 shows heat maps of these matrices obtained from the same L63 dataset used in the eigenfunction plots of Fig. 2. Similarly to (30), we form the eigenvectors $\xi_{j,z,\tau,L,N} \in \tilde{H}_N$ and $\hat{\xi}_{j,z,\tau,L,N} \in \mathcal{H}_N$ from the linear combinations

$$\xi_{j,z,\tau,L,N} = \sum_{i=1}^L (z \phi_{i,N} - \phi'_{i,N}) c_{ij}, \quad \hat{\xi}_{j,z,\tau,L,N} = \sum_{i=1}^L \sigma_{i,N} (z \varphi_{i,N} - \hat{T}_N \phi'_{i,N}) c_{ij}.$$

Moreover, similarly to $\zeta_{j,z,\tau,L,L'}$ from (31) we approximate $\hat{\zeta}_{j,z,\tau,L,N}$ by $\zeta_{j,z,\tau,L,L',N} \in \mathcal{H}_N$ using the partial isometries $T_{N,L'}: \hat{H}_N \rightarrow \mathcal{H}_N$ with $L' \leq N-1$,

$$\zeta_{j,z,\tau,L,L',N} := \sum_{i=1}^L (z \sigma_{i,N} \varphi_{i,N} - \varphi'_{i,L',N}) c_{ij}, \quad \varphi'_{i,L',N} := T_{L',N} \phi'_{i,N}.$$

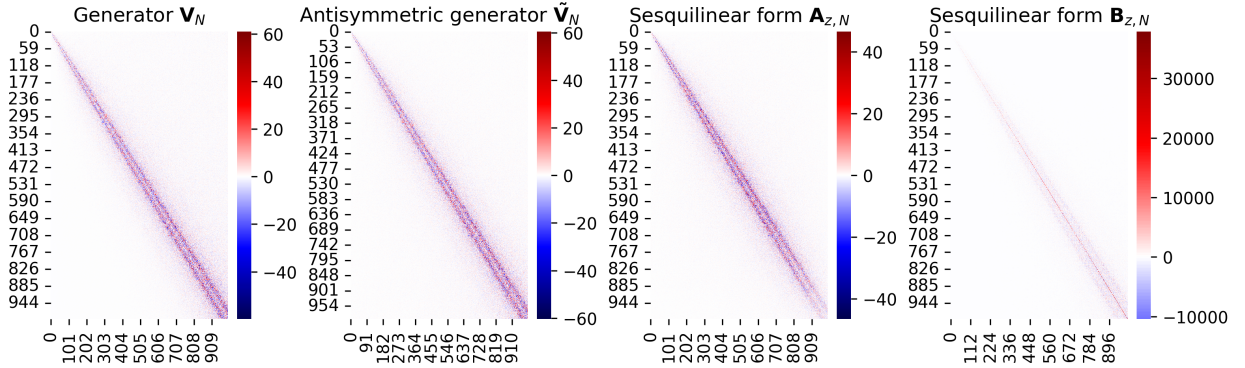


Figure 3: Matrices associated with the data-driven variational eigenvalue problem from Definition 16. From left to right, the panels show heat maps of the generator matrix \mathbf{V}_N , its antisymmetric part $\tilde{\mathbf{V}}_N$, the matrix representation $\mathbf{A}_{z,N}$ of the sesquilinear form $A_{z,N}$, and the matrix representation $\mathbf{B}_{z,N}$ of the sesquilinear form $B_{z,N}$. Matrices were computed for $L = 1000$, $z = 0.1$, and $\tau = 1 \times 10^{-5}$ using the same data and remaining parameters as the L63 experiments from Section 5.

We also note that the vectors $\xi_{j,z,\tau,L,N} \in \hat{H}_N$ have continuous representatives $\tilde{\xi}_{j,z,\tau,L,N} \in C(M)$ (cf. $\tilde{\xi}_{j,z,\tau,L}$ in (26)), where

$$\tilde{\xi}_{j,z,\tau,L,N} = \sum_{i=1}^L (z\varphi_{i,N} - \varphi'_{i,N})c_{ij}. \quad (35)$$

By (33) and property (K6), as $N \rightarrow \infty$ at fixed L , the matrices $\mathbf{A}_{\tau,N}$ and $\mathbf{B}_{z,N}$ converge to \mathbf{A}_{τ} and \mathbf{B}_z from Section 4.3, respectively, in any matrix norm. This implies convergence of eigenvalues and eigenfrequencies, $\lim_{N \rightarrow \infty} \beta_{j,z,\tau,L,N} = \beta_{j,z,\tau,L}$ and $\lim_{N \rightarrow \infty} \omega_{j,z,\tau,L,N} = \omega_{j,z,\tau,L}$, respectively, as well as convergence of the corresponding spectral projections on \mathbb{C}^L . As a result, by $C^1(M)$ -norm convergence of $\varphi_{j,\tau,N}$ to $\varphi_{j,\tau}$, we have convergence of the functions $\xi_{j,z,\tau,L,N}$ to $\xi_{j,z,\tau,L}$ in $C(M)$.

In summary, the results of the data-driven scheme described in this subsection converge to those from the Galerkin scheme of Section 4.3 as $N \rightarrow \infty$ at fixed L , and the results of the latter converge to solutions of the variational eigenvalue problem from Section 4.2 as $L \rightarrow \infty$. For completeness, we include a formula for computing the elements of the data-driven generator matrix \mathbf{V}_N ,

$$V_{ij,N} = \langle \phi_{i,N}, \tilde{K}'_N \gamma_{j,N} \rangle_N \equiv \int_X \int_X \phi_{i,N}(x) (\tilde{V}_x \cdot \hat{k}_N(x, z)) \gamma_{j,N}(z) d\mu_N(x) d\mu_N(z).$$

We see that this formula is structurally very similar to (27), with obvious replacements of analytical terms by data-driven ones. In particular, the directional derivative $\tilde{V}_x \cdot \hat{k}_N(x, z)$ of the (data-driven) kernel function \hat{k}_N is still computed with respect to the true vector field \tilde{V} . The entries $V_{ij,N}^{(2)}$ of $\mathbf{V}_N^{(2)}$ can be computed in a similar number via an analogous formula to (28). It should also be noted that when working with a pullback kernel $k^{(Y)}: Y \times Y \rightarrow \mathbb{R}$ from data space (as will be the case in the examples of Section 5), we have

$$\tilde{\xi}_{j,z,\tau,L,N} = F \circ \xi_{j,z,\tau,L,N}^{(Y)}, \quad \zeta_{j,z,\tau,L,N} = F \circ \zeta_{j,z,\tau,L,N}^{(Y)} \quad (36)$$

for everywhere-defined functions $\xi_{j,z,\tau,L,N}^{(Y)}: Y \rightarrow \mathbb{C}$ and $\zeta_{j,z,\tau,L,N}^{(Y)}: Y \rightarrow \mathbb{C}$ on data space; see Remark 4.

5. Numerical examples

We apply the spectral decomposition technique described in Section 4 to three measure-preserving ergodic systems: a linear rotation on \mathbb{T}^2 , a Stepanoff flow on \mathbb{T}^2 [36], and the L63 system on \mathbb{R}^3 [37]. The linear torus rotation is a prototypical system with pure point spectrum and analytically known Koopman eigenvalues

Table 1: Dataset attributes and numerical parameters used in the torus rotation, Stepanoff flow, and L63 experiments.

	Torus rotation	Stepanoff flow	Lorenz 63 system
Data space dimension d	4	4	3
Training samples N	60,000	68,000	80,000
Training sampling interval Δt	$\sqrt{7} \approx 2.65$	3.0	3.0
Resolvent parameter z	0.1	0.1	0.1
Regularization parameter τ	3×10^{-3}	1×10^{-6}	1×10^{-5}
Number of basis functions L, L'	400	1500	1000
Test samples \tilde{N}	2000	2000	2000
Test sampling interval $\tilde{\Delta t}$	0.01	0.01	0.01

and eigenfunctions. The Stepanoff flow has an ergodic invariant measure supported on a smooth manifold (the Lebesgue measure on the 2-torus), and is characterized by topological weak mixing, i.e., absence of nonconstant continuous Koopman eigenfunctions due to the presence of a fixed point. The L63 system has an ergodic invariant measure supported on a fractal set (the SRB measure on the Lorenz attractor), and is mixing with an associated continuous spectrum of the Koopman operator.

Our experimental setup follows closely that of [21]. In each example, we numerically generate state space trajectory data $x_0, \dots, x_{N-1} \in \mathcal{M}$, $x_n = \Phi^{n\Delta t}(x_0)$, where $\Delta t > 0$ is a fixed sampling interval and x_0 an arbitrary initial condition. We then embed the state space trajectory in data space $Y = \mathbb{R}^d$ via an embedding $F: X \rightarrow Y$ to produce time-ordered samples y_0, \dots, y_{N-1} with $y_n = F(x_n)$. The primary difference between our setup and that of [21] is that the time step Δt will be relatively large: for example, in the L63 experiments in this work we use $\Delta t = 3$, while [21] uses a significantly shorter interval $\Delta t = 0.02$ in order to approximate the Koopman resolvent by a Laplace transform. Here, we expect that this increased value of Δt will result in a more uniform sampling of the invariant measure for a given training dataset size N .

Using the samples y_n , we build Markov operators \hat{G}_N and compute their eigenvectors $\phi_{j,N}$ and corresponding eigenvalues $\lambda_{j,N}$ via the approach described in Sections 2.4 and 4.4, using a variable-bandwidth kernel $k^{(Y)}: Y \times Y \rightarrow \mathbb{R}$ of the form (B.2). We then solve the variational eigenvalue problem in Definition 16 to obtain eigenfunctions $\xi_{j,z,\tau,L,N}$ of the approximate generator $V_{z,\tau,L,N}$ and their corresponding eigenfrequencies $\omega_{j,z,\tau,L,N}$.

We order the computed eigenpairs $(\omega_{1,z,\tau,L,N}, \xi_{1,z,\tau,L,N}), (\omega_{2,z,\tau,L,N}, \xi_{2,z,\tau,L,N}), \dots$ in order of increasing Dirichlet energy $E_{j,z,\tau,L,N} := \mathcal{E}_N(\xi_{j,z,\tau,L,N})$. As discussed in Section 2.5, the Dirichlet energy measures the regularity of a given function and is larger for functions that project onto $\phi_{j,N}$ with small corresponding eigenvalues $\lambda_{j,N}$ of \hat{G}_N . The regularity measured with the Dirichlet energy can also be a useful (post-hoc) criterion for identifying spectral pollution; see [20, Corollary 3]. Alternatively, one can sort eigenfunctions in terms of the decay of their autocorrelation function as in [21], which acts as a metric of eigenfunction predictability and “closeness” to a true Koopman eigenfunction. Recall, in particular, from Section 2.2 that a Koopman eigenfunction $\xi_j \in \hat{H}$ with corresponding eigenfrequency $\omega_j \in \mathbb{R}$ will have an autocorrelation function that behaves as a pure complex phase, $C_{\xi_j \xi_j}(t) = e^{i\omega_j t}$, without amplitude decay.

Following computation of the eigenpairs $(\omega_{j,z,\tau,L,N}, \xi_{j,z,\tau,L,N})$, we build the RKHS eigenfunctions $\zeta_{j,z,\tau,L,L',N} \in \mathcal{H}_N$ and the corresponding data space functions $\zeta_{j,z,\tau,L,L',N}^{(Y)}$ using the partial isometry $T_{L,N}: \hat{H}_N \rightarrow \mathcal{H}_N$ (see Remark 4). To assess the out-of-sample behavior of our scheme, we evaluate these functions on test data $\tilde{y}_0, \dots, \tilde{y}_{N-1} \in Y$ with $\tilde{y}_n = F(\tilde{x}_n)$ obtained from a trajectory $\tilde{x}_n = \Phi^{n\tilde{\Delta t}}(\tilde{x}_0)$ with different initial condition $\tilde{x}_0 \in \mathcal{M}$ and sampling interval $\tilde{\Delta t} > 0$ to those used for the generation of the training data. We choose $\tilde{\Delta t} \ll \Delta t$ to test the ability of our scheme to reconstruct time series of observable values at high temporal resolution from temporally coarse training data.

For the remainder of this section, if there is no risk of confusion we suppress z, τ, L, L' , and N subscripts from our notation for eigenfunctions and eigenfrequencies, i.e., $\zeta_{j,z,\tau,L,L',N} \equiv \zeta_j$, $\omega_{j,z,\tau,L,N} \equiv \omega_j$, and $E_{j,z,\tau,L,N} \equiv E_j$. A summary of the dataset attributes and numerical parameters employed in our experiments is provided in Table 1.

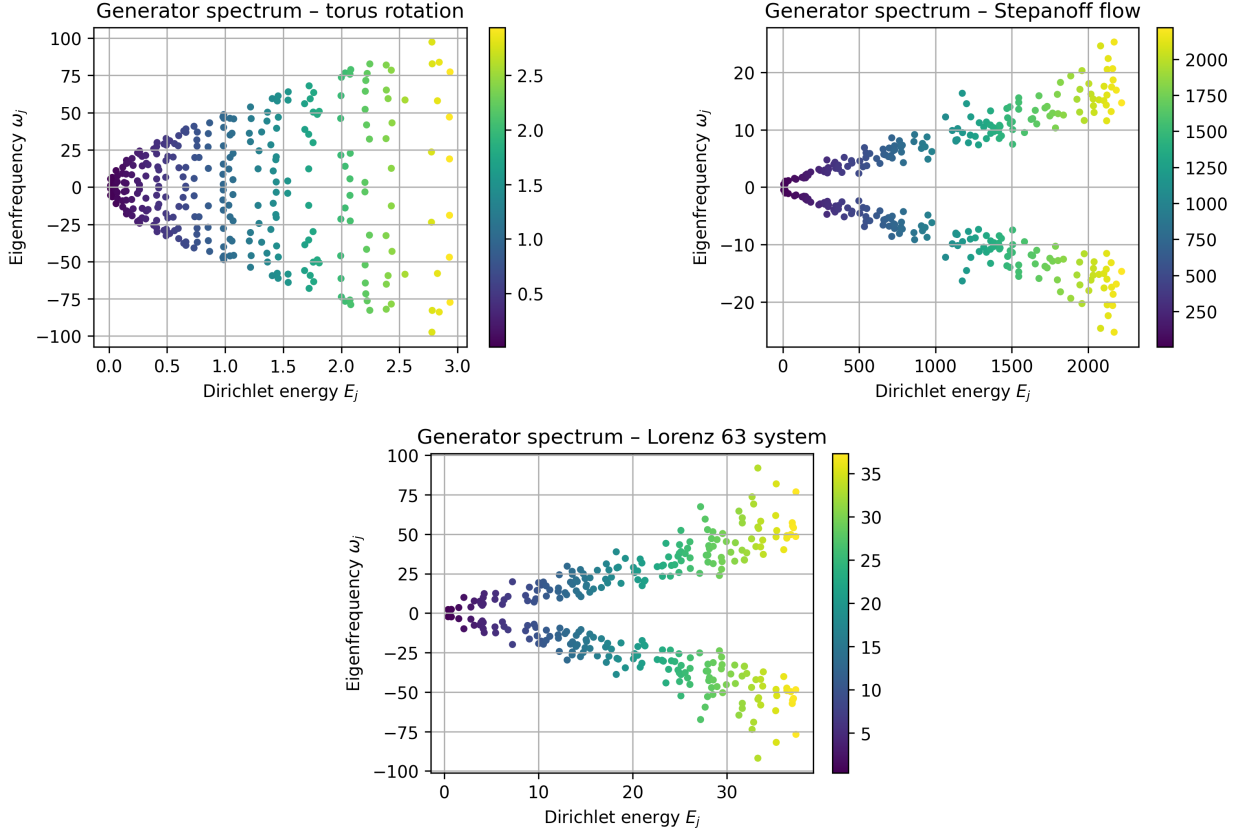


Figure 4: Regularized generator spectra for the torus rotation, Stepanoff flow, and L63 system. The plots show the first 300 eigenfrequencies ω_j , ordered in increasing order of Dirichlet energy E_j , versus E_j .

5.1. Linear torus rotation

The linear torus rotation is generated by the vector field $\vec{V}: \mathbb{T}^2 \rightarrow T\mathbb{T}^2$ with components $\vec{V}(x) = (1, \alpha)$ in canonical angle coordinates, $x = (x^1, x^2) \in [0, 2\pi)^2$, where α is an irrational frequency parameter. The resulting dynamical flow is given in closed form by $\Phi^t(x) = (x + (1, \alpha)t) \bmod 2\pi$, and has a unique ergodic invariant Borel probability measure μ given by the normalized Haar measure on \mathbb{T}^2 . Thus, in this example we have $\mathcal{M} = M = X = \mathbb{T}^2$. One readily verifies that the generator V on $H = L^2(\mu)$ is diagonal in the Fourier basis $\{\phi_l(x) = e^{il \cdot x}\}_{l \in \mathbb{Z}^2}$ of H ,

$$V\phi_l = i\alpha_l\phi_l, \quad \alpha_l = l_1 + \alpha l_2, \quad l = (l_1, l_2).$$

On the basis of these facts, our data-driven eigenfunctions ζ_j should approximate (up to a phase factor) ϕ_{l_j} for some $l_j = (l_{1j}, l_{2j}) \in \mathbb{Z}^2$ depending on the ordering ζ_1, ζ_2, \dots used. Moreover, the corresponding eigenfrequencies ω_j should be approximately equal to integer linear combinations of the basic frequencies of the rotation, $\omega_j \approx l_{1j} + l_{2j}\alpha$. As described in Section 2.2, when normalized to unit norm in H , each eigenfunction ϕ_l induces a semiconjugacy with a circle rotation of frequency α_l , and by continuity of Fourier functions that semiconjugacy is topological. This means that ζ_j should take values near the unit circle in the complex plane, and for a given initial condition $x \in \mathbb{T}^2$ the real and imaginary parts of the time series $t \mapsto \zeta_j(\Phi^t(x))$ should be sinusoids oscillating with frequency α_{l_j} and with a relative phase difference of 90° .

We compute eigenfunctions ζ_j and their corresponding eigenfrequencies ω_j using a dataset of $N = 60,000$ samples $x_n \in \mathbb{T}^2$ sampled at an interval $\Delta t = \sqrt{7} \approx 2.65$. Note that Δt sits between the slow and fast oscillation periods of the system, $2\pi/\alpha \approx 1.15 < \Delta t < 2\pi$. The dynamical states x_n are embedded in the data

space $Y = \mathbb{R}^4$ by means of the standard (flat) embedding of the 2-torus, $F(x) = (\cos x^1, \sin x^1, \cos x^2, \sin x^2)$, and we compute data-driven basis functions $\phi_{j,N}$ using the pullback kernel construction described in Section 2.4 for the data $y_n = F(x_n)$. We compute eigenpairs (ω_j, ζ_j) using $L = 400$ such basis functions and the resolvent and regularization parameters $z = 0.1$ and $\tau = 0.003$, respectively. In addition, we evaluate the continuous representatives ζ_j on a dynamical trajectory \tilde{x}_n of $\tilde{N} = 2000$ samples taken every $\tilde{\Delta t} = 0.01$ time units. Note that $\tilde{\Delta t} \ll 2\pi/\alpha$ so the out-of-sample time series $(\zeta_j(\tilde{x}_0), \zeta_j(\tilde{x}_1), \dots)$ should resolve the fast oscillatory frequency of the system as well as a number of its harmonics.

Figure 5 shows representative eigenfunction results from these computations, visualized as scatterplots of the real and imaginary parts of ζ_j on the 2-torus, traceplots of $\zeta_j(\tilde{x}_0), \zeta_j(\tilde{x}_1), \dots$ in the complex plane, and the corresponding time series of $\text{Re } \zeta_j(\tilde{x}_n)$ and $\text{Im } \zeta_j(\tilde{x}_n)$. The results are broadly consistent with the theoretical properties of Koopman eigenfunctions and eigenfrequencies mentioned above. In particular, the scatterplots of $\text{Re } \zeta_j$ and $\text{Im } \zeta_j$ (first two columns of Fig. 5 from the left) have the structure of plane waves consistent with the real and imaginary parts of Fourier functions. Moreover, the traceplots of $\zeta_j(\tilde{x}_n)$ (third column from the left) take values very close to the unit circle in \mathbb{C} , and the time series of $\text{Re } \zeta_j(\tilde{x}_n)$ and $\text{Im } \zeta_j(\tilde{x}_n)$ (rightmost column) are near-perfect sinusoids with frequencies consistent with the computed eigenfrequencies ω_j . In addition, as seen from the example of ζ_6 in the third row of Fig. 5, the numerical results well-capture the multiplicative group structure of Koopman eigenfunctions and additive group structure of the corresponding eigenfrequencies. In this case, ζ_6 exhibits a $(-1, 1)$ wavevector on the torus, and this is consistent with the product $\zeta_1 \zeta_3$ between eigenfunctions ζ_1 and ζ_3 (with wavevectors $(-1, 0)$ and $(0, 1)$, respectively) shown in the first two rows. The corresponding eigenfrequency, $\omega_6 \approx 4.50$, is also consistent with $\omega_1 + \omega_3 \approx -1.00 + 5.49$ to two significant digits.

In closing this subsection, we note that despite the highly structured nature of this system, accurate numerical spectral decompositions of the generator is non-trivial in approximation spaces of high dimension (here, L) since the point spectrum $\sigma_p(V) = \{i(l_1 + l_2\alpha)\}_{l_1, l_2 \in \mathbb{Z}}$ is a dense subset of the imaginary line. Indeed, see the top row in [20, Figure 5] for an illustration of poor numerical performance of a naive approximation scheme for the generator as L increases at fixed N without using regularization.

5.2. Stepanoff flow

Our next example comes from a class of Stepanoff flows on the 2-torus studied by [36]. The dynamical vector field $\vec{V}: \mathbb{T}^2 \rightarrow \mathbb{T}^2$ has the coordinate representation $\vec{V}(x) = (V^1(x), V^2(x))$, where

$$V^1(x) = V^2(x) + (1 - \alpha)(1 - \cos x^2), \quad V^2(x) = \alpha(1 - \cos(x^1 - x^2)), \quad (37)$$

$x = (x^1, x^2) \in [0, 2\pi)^2$ and α is a real parameter. The Stepanoff vector field \vec{V} has zero divergence with respect to the Haar measure μ ,

$$\text{div}_\mu \vec{V} = \frac{\partial V^1}{\partial x^1} + \frac{\partial V^2}{\partial x^2} = 0,$$

which implies that μ is an invariant measure under the associated flow Φ^t . Thus, we have $\mathcal{M} = M = X = \mathbb{T}^2$ as in the linear rotation example from Section 5.1. Still, a major difference between the linear torus rotation and the Stepanoff flow is that the latter exhibits a fixed point at $x = 0$, $\vec{V}(0) = 0$. In [36] it is shown that the normalized Haar measure is the unique invariant Borel probability measure of this flow that assigns measure 0 to the singleton set $\{0\} \subset \mathbb{T}^2$ containing the fixed point.

Since any continuous, non-constant Koopman eigenfunction induces a semiconjugacy with a circle rotation of nonzero frequency, the existence of the fixed point at $x = 0$ implies that the system has no continuous Koopman eigenfunctions; i.e., it is topologically weak-mixing. In fact, [36] shows that when α is irrational the Stepanoff flow is topologically conjugate to a time-reparameterized irrational rotation on \mathbb{T}^2 with frequency parameters $(1, \alpha)$, for a time-reparameterization function that is singular at $x = 0$. There are many examples of time-reparameterizations of pure-point-spectrum systems that yield measure-theoretically mixing dynamics [38, 39], including examples on tori [40]. While, to our knowledge, and there are no results in the literature on the measure-theoretic mixing properties of Stepanoff flows, these considerations on time reparameterization in conjunction with the singularity of the time-parameterization function at

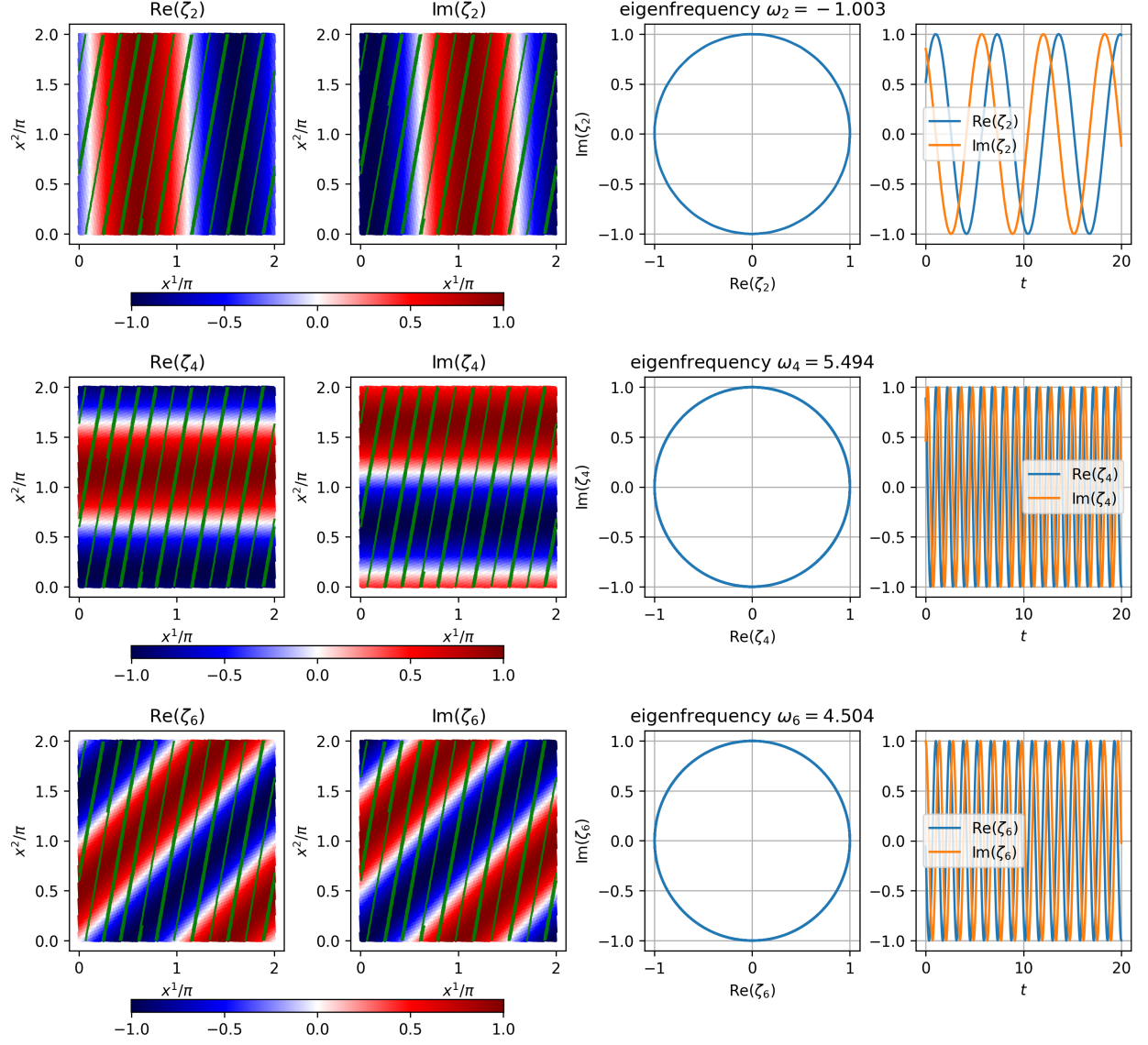


Figure 5: Representative generator eigenfunctions ζ_j for the linear torus rotation. In each row, the first two panels from the left show scatterplots of the real and imaginary parts of $\zeta_j(x_n)$ on the training data $x_n \in \mathbb{T}^2$. The third and fourth panels show the evolution of $\zeta_j(\tilde{x}_n)$ in the complex plane and time series of corresponding real and imaginary parts, sampled along the test trajectory \tilde{x}_n . The test trajectory \tilde{x}_n is plotted with green lines in the first two panels for reference.

$x = 0$ suggest that the Koopman operator for the Stepanoff flow on $H = L^2(\mu)$ has non-trivial continuous spectrum. At the very least, the absence of continuous Koopman eigenfunctions implies that data-driven spectral computations are non-trivial for this class of systems even if eigenfunctions exist in $L^2(\mu)$.

Similarly to the linear rotation experiments from Section 5.1, we generate training data $y_n \in \mathbb{R}^4$ by embedding discrete-time samples $x_n \in \mathbb{T}^2$ of a dynamical trajectory under the Stepanoff flow using the flat embedding $F: \mathbb{T}^2 \rightarrow \mathbb{R}^4$. In this case, the flow Φ^t is not available analytically, so we compute the x_n by numerical solution of the initial-value problem (2). We generate $N = 68,000$ samples at a sampling interval $\Delta t = 3.0$. Using those samples, we compute basis functions $\phi_{j,N}$ as in Section 5.1 and generator eigenpairs (ω_j, ζ_j) using $L = 1500$ basis functions and the parameters $z = 0.1$, $\tau = 1 \times 10^{-6}$. We again generate a test dataset \tilde{x}_n of $\tilde{N} = 2000$ samples taken on a dynamical trajectory, which independent of the training data every. The samples are taken at $\Delta t = 0.01$ time units and we evaluate the continuous functions ζ_j on that dataset.

Figure 6 shows generator eigenfunction results obtained from these experiments. The layout of the plots is similar to that of the torus rotation results in Fig. 5. We see that despite the non-integrable nature of the dynamics, the depicted eigenfunctions ζ_j exhibit an approximate form of cyclicity. Particular eigenfrequencies, e.g., $\omega_{21} \approx 2.10$ appear to be approximate harmonics of a basic frequency $\omega_3 \approx 1.03$. The level sets of the real and imaginary parts of the corresponding eigenfunctions ζ_j exhibit characteristic “S-shaped” patterns that are broadly aligned with the dynamical flow (see the second and third rows from the top in Fig. 6).

A notable feature of these patterns is smaller-scale oscillations near the fixed point at 0; this is particularly evident for the higher-frequency eigenfunction ζ_{97} shown in the bottom row of the figure. The presence of these small-scale oscillations is qualitatively consistent with the slowing down of the dynamical flow near the fixed point. In particular, an orbit passing through a region near the fixed point has to cross more eigenfunction wavefronts in a given time interval to produce consistent phase evolution $\zeta_j(\Phi^t(x)) \approx e^{i\omega_j t} \zeta_j(x)$ with more rapidly evolving orbits away from the fixed point.

Meanwhile, the leading nonconstant eigenfunction with respect to the Dirichlet energy ordering, ζ_1 , displayed in the top row of Fig. 6, exhibits a similar S-shaped structure with weaker spatial variability near the fixed point and a correspondingly smaller eigenfrequency $\omega_1 \approx 0.49$. The corresponding time series exhibit oscillatory behavior that is generally consistent with a periodicity of $2\pi/\omega_1 \approx 12.8$, but the dominant low-frequency oscillations are evidently mixed with higher-frequency components.

As a final remark on the Stepanoff experiments, we mention that besides eigenfunctions such as ζ_1 , ζ_3 , and ζ_{21} (whose level sets are predominantly aligned with the dynamical flow), the numerical generator spectrum contains other eigenfunctions, e.g., ζ_{78} in the bottom row of Fig. 6, featuring oscillations transverse to the flow and approximately cyclical time series behavior.

5.3. Lorenz 63 system

Our third numerical example is the L63 system on \mathbb{R}^3 , generated by the vector field $\vec{V}: \mathbb{R}^3 \rightarrow T\mathbb{R}^3 \cong \mathbb{R}^3$, where

$$\vec{V}(x) = (V^1(x), V^2(x), V^3(x)) = (-\sigma(x^2 - x^1), x^1(\rho - x^3) - x^2, x^1x^2 - \beta x^3) \quad (38)$$

and $x = (x^1, x^2, x^3)$. We use the standard parameter values $\beta = 8/3$, $\rho = 28$, $\sigma = 10$, and the identity for the observation map $F: \mathbb{R}^3 \rightarrow \mathbb{R}^3$. For this choice of parameters, the L63 system is known to have a compact attractor $X \subset \mathbb{R}^3$ with fractal dimension ≈ 2.06 that supports a unique (and observable) SRB measure μ [16]. The system is also known to be mixing with respect to μ [17], which implies that the associated unitary group of Koopman operators U^t has no nonzero eigenfrequencies. The H_p subspace is then a one-dimensional space of constant functions, while H_c contains all zero-mean functions in $L^2(\mu)$ (i.e., $H_c = \tilde{H}$; see Section 2.2).

The L63 system with the standard parameter values is dissipative with respect to Lebesgue measure, $\text{div}_{\text{Leb}} \vec{V} = \sum_{i=1}^3 \frac{\partial V^i}{\partial x^i} < 0$, and can be shown to possess compact absorbing balls containing X [41]. Setting the forward-invariant manifold M to such an absorbing ball, we have $X \subset M \subset \mathcal{M} = \mathbb{R}^3$ and properties (K1)–(K6) are all rigorously satisfied. Compared to the linear rotation and Stepanoff flow, where the support of the invariant measure μ is a smooth manifold, $X = \mathbb{T}^2$, a challenging aspect of the L63 system

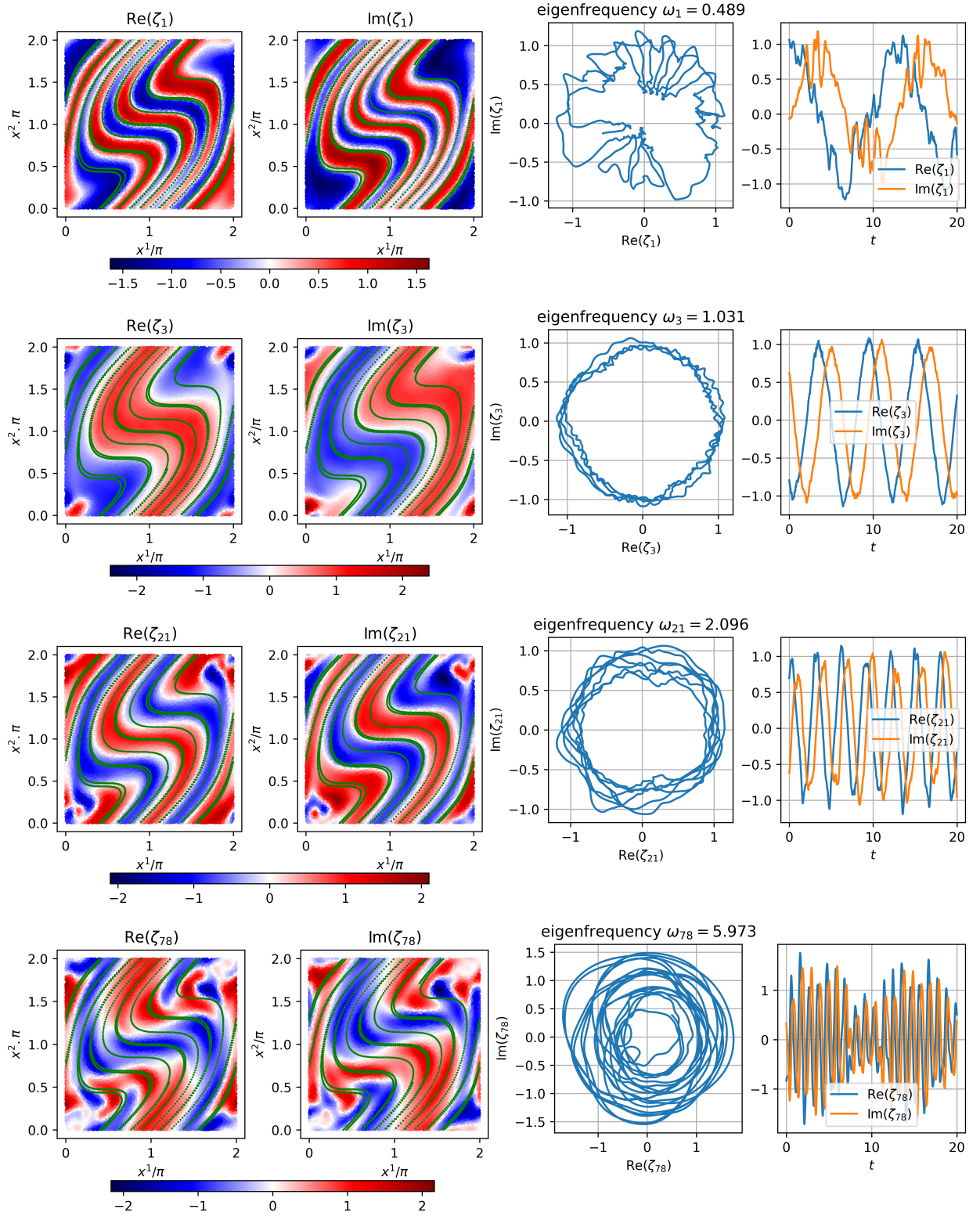


Figure 6: As in Fig. 5, but for regularized generator eigenfunctions for the Stepanoff flow.

is that μ is supported on a fractal set. The kernel eigenbasis $\phi_{j,N}$, provides an effective way of building Galerkin approximation spaces in such settings with invariant measures supported on geometrically complex sets.

In this example, we use a training dataset consisting of $N = 80,000$ samples $y_n = x_n \in \mathbb{R}^3$ which are taken at a sampling interval of $\Delta t = 3$ time units from a numerical trajectory that was allowed to equilibrate near the Lorenz attractor. Note that Δt is significantly longer than the Lyapunov timescale $1/\Lambda \approx 1.10$, where $\Lambda \approx 0.91$ is the positive Lyapunov exponent of the L63 system for the standard parameter values [42]. As a result, we expect the training samples x_n to exhibit a degree of statistical independence. Using this dataset, we compute generator eigenpairs (ω_j, ζ_j) using $L = 1000$ basis functions $\phi_{j,N}$ and the parameters $z = 0.1$ and $\tau = 1 \times 10^{-5}$. As in Sections 5.1 and 5.2, we generate a test dataset $\tilde{y}_n = \tilde{x}_n$ of $\tilde{N} = 2000$ samples at higher temporal resolution $\tilde{\Delta t} = 0.01$, and we evaluate the continuous functions ζ_j on the \tilde{x}_n data.

Figure 7 shows representative eigenfunction results obtained from these experiments, visualized as scatterplots on the Lorenz attractor (first and second columns from the left), traceplots in the complex plane (third column from the left), and time series plots of the real and imaginary parts of ζ_j (rightmost column). Despite the mixing nature of the dynamics, the extracted eigenfunctions exhibit approximate cyclicity that persists on significantly longer timescales than the Lyapunov timescale of the system. One of these eigenfunctions, ζ_{32} (second row in Fig. 7), with corresponding eigenfrequency $\omega_j \approx 8.46$, shows a characteristic “wavenumber-1” pattern on the lobes on the attractor that qualitatively resembles results obtained by several other methods; see, e.g., [43, 20, 11, 21, 44]. Other results in Fig. 7 include eigenfunction ζ_{100} (bottom row) with a corresponding eigenfrequency $\omega_{100} \approx 16.8$ that appears to be a “wavenumber-2” harmonic of ζ_{32} . Additionally, the eigenfunction ζ_{63} (third row) has an eigenfrequency $\omega_{63} \approx 15.9$ that is also close to $2\omega_{32}$ but exhibits smaller-scale oscillations along the radial directions of the attractor lobes. As a lower-frequency example, eigenfunction ζ_1 (top row), has an eigenfrequency of $\omega_1 \approx -2.23$ and a corresponding oscillatory timescale of $2\pi/|\omega_1| \approx 2.78$ that is approximately 2.5 times longer than the Lyapunov timescale. Capturing such low-frequency coherent patterns is challenging with data-driven techniques, as evidenced by the noisier nature of the time series plots in the top row of Fig. 7. Nonetheless, the evolution of ζ_1 is predominantly cyclical.

6. Concluding remarks

We have proposed a data-driven technique for spectral approximation of Koopman operators of continuous-time, measure-preserving, ergodic dynamical systems. A key feature of this method is that it is physics-informed, in the sense that it makes use of known equations of motion through the dynamical vector field without requiring access to pairs of snapshot data to approximate the Koopman operator. Another primary element is a bounded transformation of the Koopman generator, V , that renders it into a skew-adjoint operator that is amenable to compact approximations by smoothing with Markovian kernel integral operators. This leads to a two-parameter family $V_{z,\tau}$, $z, \tau > 0$, of skew-adjoint operators on L^2 with compact resolvent, and thus with a discrete spectrum consisting entirely of eigenvalues and an associated orthonormal basis of eigenfunctions. Our main theoretical result, Theorem 2, established spectral convergence of the family $V_{z,\tau}$ to the generator V in the iterated limit of $z \rightarrow 0^+$ after $\tau \rightarrow 0^+$. The approximation of these operators in the data-driven setting converges in four successive limits: namely that of the number of data snapshots $N \rightarrow \infty$, basis functions $L \rightarrow \infty$, smoothing parameter $\tau \rightarrow 0^+$, and resolvent parameter $z \rightarrow 0^+$. In the discrete-time setting it has been shown that three successive limits are required for consistent spectral approximation of unitary Koopman operators of measure-preserving systems [45]. The use of iterated limits is thus likely to be necessary when accurately computing the spectrum of Koopman generators. Compared to our previous work, the physics-informed approach presented in this paper avoids having to take a limit of vanishing sampling interval, $\Delta t \rightarrow 0^+$, needed for finite-difference approximation of the generator [20] or approximation of the Koopman resolvent via a Laplace transform [21].

In addition, we have shown that the eigendecomposition of $V_{z,\tau}$ can be formulated as a generalized eigenvalue problem involving V and the Markov smoothing operators. We developed variational Galerkin

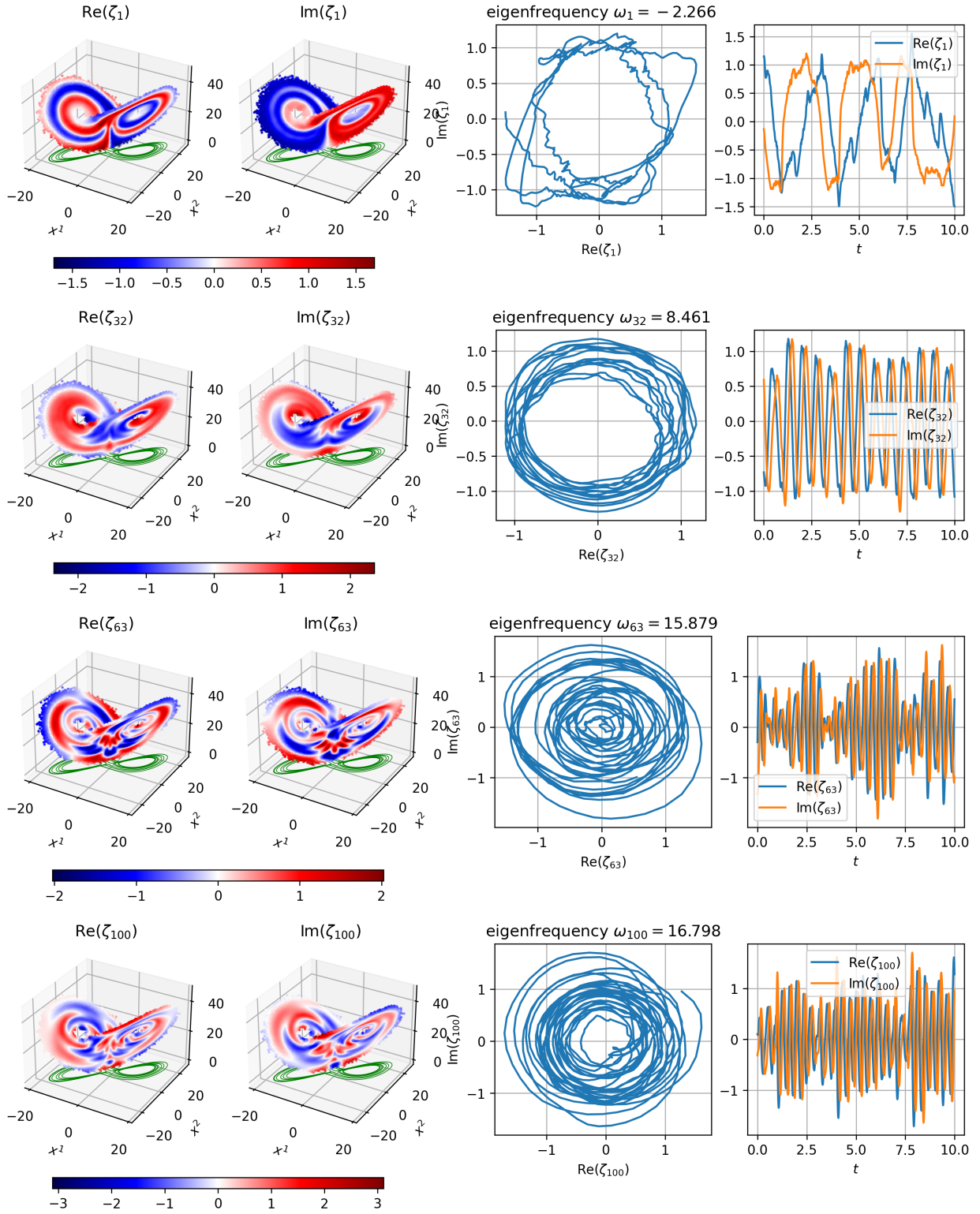


Figure 7: As in Fig. 5, but for regularized generator eigenfunctions for the L63 system.

methods for approximating solutions of this problem in finite-dimensional spaces spanned by kernel eigenfunctions. A noteworthy aspect of these approximation schemes is that they employ automatic differentiation to evaluate the action of the dynamical vector field on kernel functions, thus making direct use of equations of motion. Moreover, as with other kernel methods, these numerical schemes are well-suited for handling invariant measures supported on geometrically complex sets (e.g., fractal attractors) and/or measures with supports embedded in high-dimensional ambient data spaces. In particular, our usage of kernel integral operators serves the dual purpose of basis learning for Galerkin approximation and smoothing for spectral regularization of the generator.

The eigenfunctions of $V_{z,\tau}$ can be interpreted as generalizations of Koopman eigenfunctions of pure point spectrum systems, in the sense of providing an orthonormal basis of L^2 that contains elements with approximately cyclical behavior and slow decay of correlations. In addition, every eigenfunction in our construction has a representative in an RKHS of continuously differentiable functions, allowing out-of-sample evaluation by means of Nyström operators that can be used, e.g., to reconstruct eigenfunction time series at high temporal resolution from coarsely sampled (in time) training data. We have demonstrated these features through a suite of numerical experiments involving low-dimensional systems with different spectral characteristics: (i) an ergodic torus rotation as a prototypical system with pure point spectrum; (ii) a Stepanoff flow on the 2-torus as an example with topological weak mixing (absence of continuous Koopman eigenfunctions) and smooth invariant measure; and (iii) the L63 system as an example with measure-theoretic mixing and invariant measure supported on a fractal set.

In terms of future work, it would be interesting to characterize limits of the eigenfunctions of $V_{z,\tau}$ in a space of distributions such as H^{-1} (see Section 2.5), similarly to the analysis of [44] for unitary Koopman operators. Another possible direction would be to employ the eigendecomposition of $V_{z,\tau}$ in supervised learning schemes for the Koopman evolution of observables.

Acknowledgments

Dimitrios Giannakis acknowledges support from the US Office of Naval Research under MURI grant N00014-19-1-242, and the US Department of Defense, Basic Research Office under Vannevar Bush Faculty Fellowship grant N00014-21-1-2946. Claire Valva was supported by the US National Science Foundation Graduate Research Fellowship under grant DGE-1839302. The authors declare no competing interests.

Code availability

Python code reproducing the numerical results in this paper is available at the repository <https://github.com/dg227/NLSA> under directory `Python/examples/resolvent_compactification`.

Appendix A. Auxiliary results

Appendix A.1. Proof of Proposition 14.

First, note that when implemented with a data-adapted kernel k such as the variable-bandwidth Gaussian kernel (B.2), the bistochastic normalization procedure described in Section 2.4 may start from a data-dependent kernel $k_N: \mathcal{M} \times \mathcal{M} \rightarrow \mathbb{R}$ approximating k ; e.g.,

$$k_N(x, y) = \exp \left(-\frac{\|x - y\|^2}{\epsilon^2 \rho_N(x) \rho_N(y)} \right), \quad (\text{A.1})$$

where $\rho_N: \mathcal{M} \rightarrow \mathbb{R}$ is a data-driven approximation of the bandwidth function ρ in (B.2). For simplicity of exposition, in what follows we prove Proposition 14 for a fixed, data-independent kernel k whose restriction on $M \times M$ is C^1 . A similar method of proof can be employed for data-dependent kernels k_N that converge to k as $N \rightarrow \infty$ in $C^1(M \times M)$ norm. This will hold, for instance, in the case of (A.1) where the bandwidth functions ρ_N are built using kernel density estimation with C^1 kernels; see [46, 20] for further details.

In the following, $C(M, T^*M)$ will denote the Banach space of continuous dual vector fields on M (sections of the cotangent bundle T^*M), equipped with the norm $\|\alpha\|_{C(M, T^*M)} = \|x \mapsto \|\alpha(x)\|_{T_x^*M}\|_{C(M)}$. Here, $\|\cdot\|_{T_x^*(M)}$ is the norm on the dual tangent space T_x^*M at $x \in M$ induced by some C^1 Riemannian metric on M (all such choices of metric yield equivalent norms by compactness of M). Letting also $d: C^1(M) \rightarrow C(M, T^*M)$ denote the exterior derivative, we can define the $C^1(M)$ norm on functions as

$$\|f\|_{C^1(M)} = \|f\|_{C(M)} + \|df\|_{C(M, T^*M)}. \quad (\text{A.2})$$

With $\kappa \in C^1(M \times M)$ and ν a Borel probability measure, we let $I_{\kappa, \nu}: C(M) \rightarrow C^1(M)$ be the integral operator defined as $I_{\kappa, \nu}f = \int_M \kappa(\cdot, x)f(x) d\nu(x)$ and $\mathfrak{d}_\kappa \in C(M \times M)$ the positive, continuous function $\mathfrak{d}_\kappa(x, y) = \|d_x \kappa(\cdot, y)\|_{T_x^*(M)}$. Using (A.2), we get the following bound for the C^1 norm of $I_{\kappa, \nu}f$ that will be useful below,

$$\begin{aligned} \|I_{\kappa, \nu}f\|_{C^1(M)} &= \|I_{\kappa, \nu}f\|_{C(M)} + \|dI_{\kappa, \nu}f\|_{C(M, T^*M)} \\ &\leq \|\kappa\|_{C(M \times M)} \|f\|_{C(M)} + \|\mathfrak{d}_\kappa\|_{C(M \times M)} \|f\|_{C(M)} \\ &= \|\kappa\|_{C^1(M \times M)} \|f\|_{C(M)}. \end{aligned} \quad (\text{A.3})$$

We also define the covector-field-valued integral operator $I_{d\kappa, \nu}: C(M) \rightarrow C(M, T^*M)$ as

$$I_{d\kappa, \nu}f = \int_M d\kappa(\cdot, x)f(x) d\nu(x).$$

Next, let $\mathbb{E}_\nu f = \int_M f d\nu$ denote the expectation of $f \in C(M)$ with respect to a Borel probability measure ν on M . Following [35], we will employ the notion of Glivenko–Cantelli classes to identify sets of functions with uniform convergence of ergodic averages.

Definition 17. Let ν_N be a sequence of Borel probability measures that converges, as $N \rightarrow \infty$, to ν in weak-* sense. A set $\mathcal{G} \subseteq C(M)$ is said to be a Glivenko–Cantelli class with respect to ν_N and ν if $\lim_{N \rightarrow \infty} \sup_{g \in \mathcal{G}} |\mathbb{E}_{\nu_N} g - \mathbb{E}_\nu g| = 0$.

If $\kappa: \mathcal{M} \times \mathcal{M} \rightarrow \mathbb{R}$ and $f: M \rightarrow \mathbb{R}$ are continuous, it can be shown by results of [35] that the set $\mathcal{G}_{\kappa, f} = \{\kappa(x, \cdot)f : x \in M\}$ is Glivenko–Cantelli with respect to the invariant measure μ and sampling measures μ_N . For a compact manifold M , $\mathcal{G}_{d\kappa, f} = \{y \mapsto d_x \kappa(\cdot, y)f(y) : x \in M\}$ can also be shown to be a Glivenko–Cantelli class within $C(M, T^*M)$. We then have:

Lemma 18. Let $\kappa_N \in C^1(M \times M)$ and $f_N \in C(M)$ be sequences of kernels and functions converging to $\kappa \in C^1(M \times M)$ and $f \in C(M)$, respectively, as $N \rightarrow \infty$. Then, $g_N = I_{\kappa_N, \mu_N} f_N$ converges to $g = I_{\kappa, \mu} f$ in $C^1(M)$.

Proof. We split the estimate for $\|g_N - g\|_{C^1(M)}$ into three terms,

$$\|g_N - g\|_{C^1(M)} \leq T_{1,N} + T_{2,N} + T_{3,N},$$

where

$$\begin{aligned} T_{1,N} &= \|I_{\kappa_N, \mu_N} f_N - I_{\kappa, \mu_N} f_N\|_{C^1(M)}, \\ T_{2,N} &= \|I_{\kappa, \mu_N} f_N - I_{\kappa, \mu_N} f\|_{C^1(M)}, \\ T_{3,N} &= \|I_{\kappa, \mu_N} f - I_{\kappa, \mu} f\|_{C^1(M)}. \end{aligned}$$

We can estimate $T_{1,N}$ and $T_{2,N}$ using (A.3) as

$$\begin{aligned} T_{1,N} &= \|(I_{\kappa_N} - I_{\kappa, \mu_N})f_N\|_{C^1(M)} \leq \|\kappa_N - \kappa\|_{C^1(M \times M)} \|f_N\|_{C(M)}, \\ T_{2,N} &= \|I_{\kappa, \mu_N}(f_N - f)\|_{C^1(M)} \leq \|\kappa\|_{C^1(M \times M)} \|f_N - f\|_{C(M)}, \end{aligned}$$

and we deduce that $\lim_{N \rightarrow \infty} T_{1,N} = \lim_{N \rightarrow \infty} T_{2,N} = 0$ from the facts that $\lim_{N \rightarrow \infty} \|\kappa_N - \kappa\|_{C^1(M \times M)} = 0$ and $\lim_{N \rightarrow \infty} \|f_N - f\|_{C(M)} = 0$. For $T_{3,N}$, we have

$$T_{3,N} = \|I_{\kappa, \mu_N} f - I_{\kappa, \mu} f\|_{C(M)} + \|I_{d\kappa, \mu_N} f - I_{d\kappa, \mu} f\|_{C(M, T^*M)},$$

and it follows that $\lim_{N \rightarrow \infty} T_{3,N} = 0$ since $\mathcal{G}_{\kappa, f}$ and $\mathcal{G}_{d\kappa, f}$ are Glivenko–Cantelli classes. \square

We will now use Lemma 18 repeatedly to prove the proposition.

First, consider the normalization procedure used to construct the asymmetric kernel function $\hat{k}_N: \mathcal{M} \times \mathcal{M} \rightarrow \mathbb{R}$ (the data-driven analog of \hat{k} from (7)):

$$d_N = \int_M k(\cdot, x) d\mu_N(x), \quad q_N = \int_M \frac{k(\cdot, x)}{d_N(x)} d\mu_N(x), \quad \hat{k}_N(x, y) = \frac{k(x, y)}{d_N(x)q_N^{1/2}(y)}.$$

Applying Lemma 18 for $\kappa = k$ and $f_N = \mathbf{1}$, it follows that d_N converges to d in $C^1(M)$, and so does $1/d_N$ to $1/d$ since $1/d$ is strictly positive on the compact manifold M . Thus, from Lemma 18 with $\kappa = k$ and $f_N = 1/d_N$, we get $C^1(M)$ convergence of q_N to q . We therefore deduce $C^1(M \times M)$ convergence of \hat{k}_N to \hat{k} .

Consider now the integral operators $\hat{K}_N: \hat{H}_N \rightarrow C^1(M)$, $\hat{K}_N^\top: \hat{H}_N \rightarrow C^1(M)$, and $\tilde{K}_N: \hat{H}_N \rightarrow \hat{H}_N$, where

$$\hat{K}_N f = \int_M \hat{k}_N(\cdot, x) f(x) d\mu_N(x), \quad \hat{K}_N^\top f = \int_M \hat{k}_N(x, \cdot) f(x) d\mu_N(x),$$

and $\tilde{K}_N = \iota_N \hat{K}_N$. Consider also an SVD of \tilde{K}_N ,

$$\tilde{K}_N = \sum_{j=0}^{N-1} \phi_{j,N} \sigma_{j,N} \langle \gamma_{j,N}, \cdot \rangle_N$$

where $\sigma_{j,N} \geq 0$ are singular values, and $\{\phi_{j,N}\}_{j=0}^{N-1}$ and $\{\gamma_{j,N}\}_{j=0}^{N-1}$ are orthonormal bases of \hat{H}_N consisting of left and right singular vectors, respectively. Since $\tilde{K}_N \tilde{K}_N^* \equiv G_N$ and $\tilde{K}_N^* \tilde{K}_N$ converge spectrally to $\tilde{K} \tilde{K}^* \equiv G$ and $\tilde{K}^* \tilde{K}$, respectively, for every $j \in \mathbb{N}$ there exists $N_* > 0$ such that, by strict positivity of σ_j , $\sigma_{j,N} > 0$ for all $N > N_*$. For every such N , the corresponding singular vectors $\phi_{j,N}$ and $\gamma_{j,N}$ have $C^1(M)$ representatives

$$\varphi_{j,N} = \frac{1}{\sigma_{j,N}} \hat{K}_N \gamma_{j,N}, \quad \tilde{\gamma}_{j,N} = \frac{1}{\sigma_{j,N}} \hat{K}_N^\top \phi_{j,N}.$$

Moreover, for every choice of left and right singular vectors ϕ_j and γ_j of \hat{K} corresponding to σ_j , with continuous representatives φ_j and $\tilde{\gamma}_j$, respectively, there exist sequences $(\phi_{j,N})_N$ and $(\gamma_{j,N})_N$ of left and right singular vectors of \tilde{K}_N such that $\lim_{N \rightarrow \infty} \varphi_{j,N} = \varphi_j$ and $\lim_{N \rightarrow \infty} \tilde{\gamma}_{j,N} = \tilde{\gamma}_j$ in $C(M)$. Here, $\tilde{\gamma}_j$ is the continuous representative of γ_j defined analogously to $\tilde{\gamma}_{j,N}$ using an integral operator $\hat{K}^\top: H \rightarrow C^1(M)$.

We complete the proof by verifying that the convergence of $\tilde{\varphi}_{j,N}$ to φ_j is, in fact, in $C^1(M)$ norm. Indeed, since

$$\varphi_{j,N} = \frac{1}{\sigma_{j,N}} \int_M \hat{k}_N(\cdot, x) \gamma_{j,N}(x) d\mu_N(x) = \frac{1}{\sigma_{j,N}} \int_M \hat{k}_N(\cdot, x) \tilde{\gamma}_{j,N}(x) d\mu_N(x) = \frac{1}{\sigma_{j,N}} I_{\hat{k}_N, \mu_N} \tilde{\gamma}_{j,N},$$

it follows from Lemma 18 with $\kappa = \hat{k}_N$ and $f_N = \tilde{\gamma}_{j,N}$, and the fact that $\sigma_{j,N} \rightarrow \sigma_j$, that $\varphi_{j,N}$ converges to φ_j in $C^1(M)$, proving the proposition.

Appendix A.2. Results from the Borel functional calculus

Let \mathbb{H} be a Hilbert space, Σ a σ -algebra on a set \mathbb{X} , and $E: \Sigma \rightarrow B(H)$ a PVM. We recall the following standard results from the Borel functional calculus [e.g., 47]:

- For every $f \in \mathbb{H}$, the map $E_f: \Sigma \rightarrow \mathbb{R}_+$ with $E_f(S) = \langle f, E(S)f \rangle_{\mathbb{H}}$ is a positive finite measure.

- For every bounded Σ -measurable function $g: \mathbb{X} \rightarrow \mathbb{C}$ and every $f \in \mathbb{H}$, we have $\|Gf\|_{\mathbb{H}}^2 = \int_{\mathbb{X}} |g|^2 dE_f$, where $G = \int_{\mathbb{X}} g dE$.

The following lemma is used in the proof of Theorem 5.

Lemma 19. *Let $A: D(A) \rightarrow \mathbb{H}$ be a self-adjoint operator on a Hilbert space \mathbb{H} with associated PVM $E: \mathcal{B}(\mathbb{R}) \rightarrow B(\mathbb{H})$. Then, for every bounded Borel-measurable function $g: \mathbb{R} \rightarrow \mathbb{C}$ and Borel-measurable set $S \subseteq \mathbb{R}$, we have $\|G_S f\|_{\mathbb{H}} \leq \|g\|_{\infty} \sqrt{E_f(S)}$, where $G_S = \int_{\mathbb{S}} g dE$.*

Proof. We have $G_S = g_S(A)$, where $g_S = \chi_S g$ and $\chi_S: \mathbb{R} \rightarrow \mathbb{R}$ is the characteristic function of S . Then, by the properties of the Borel functional calculus listed above, we get

$$\|G_S f\|_{\mathbb{H}}^2 = \int_{\mathbb{X}} |g_S|^2 dE_f \leq \|g_S\|_{\infty}^2 E_f(S) \leq \|g\|_{\infty}^2 E_f(S). \quad \square$$

Appendix B. Variable-bandwidth kernels

Here, we briefly describe the construction of the variable-bandwidth kernels employed for the numerical experiments in Section 5. In the applications that we consider, the state space \mathcal{M} is embedded in a data space Y by means of a map $F: \mathcal{M} \rightarrow Y$. We assume that Y has an appropriate differentiable structure such that the restriction of F onto M is C^1 . In this scenario, it is natural to work with kernels k obtained by pullbacks of kernels $k^{(Y)}: Y \times Y \rightarrow \mathbb{R}$ on data space, i.e., $k(x, y) = k^{(Y)}(F(x), F(y))$. As a concrete example, we mention the Gaussian radial basis function (RBF) kernel on $Y = \mathbb{R}^d$,

$$k^{(Y)}(x, y) = k_{\epsilon}^{\text{RBF}}(x, y) \equiv e^{-\|x-y\|^2/\epsilon^2}, \quad (\text{B.1})$$

where $\|\cdot\|$ is the Euclidean 2-norm and $\epsilon > 0$ a bandwidth parameter.

In the experiments of Section 5 we use a variable-bandwidth generalization [48] of the Gaussian RBF, given by

$$k^{(Y)}(x, y) = \exp\left(-\frac{\|x-y\|^2}{\epsilon^2 r(x)r(y)}\right). \quad (\text{B.2})$$

Here, $r \in C^1(Y)$ is a strictly positive bandwidth function designed to take large (small) values in regions of small (large) sampling density of the data relative to Lebesgue measure on data space. In this paper, we employ the bandwidth function $r(x) = \rho_N^{-1/m}(x)$, where $m \in \mathbb{R}$ is a numerically computed dimension parameter for the support of μ , and ρ_N is a density function given by

$$\rho_N(x) = \int_M \bar{p}_N(x, y) d\mu_N(y)$$

for a Markov kernel $\bar{p}_N: M \times M \rightarrow \mathbb{R}$. Setting $\bar{k}(x, y) = k_{\bar{\epsilon}}^{\text{RBF}}(F(x), F(y))$ for a bandwidth parameter $\bar{\epsilon}$ independent from ϵ , we build \bar{p}_N by applying to \bar{k} the normalization procedure introduced in the diffusion maps algorithm [49]:

$$\bar{p}(x, y) = \frac{\bar{k}(x, y)}{\bar{d}_N(x)\bar{q}_N(x)\bar{q}_N(y)}, \quad d_N(x) = \int_M \frac{\bar{k}(x, y)}{\bar{q}_N(x)\bar{q}_N(y)} d\mu_N(y), \quad \bar{q}_N(x) = \int_M \bar{k}(x, y) d\mu_N(y).$$

Moreover, we tune the bandwidth parameters ϵ and $\bar{\epsilon}$ automatically using a variant of a procedure proposed by [50]. This procedure also yields the dimension parameter m .

With this choice of kernel \bar{p}_N , if μ is a smooth measure supported on a Riemannian manifold then ρ_N approximates the density of μ relative to the Riemannian volume measure. It can be shown (e.g., [46]) that as $\bar{\epsilon}$ and ϵ become small, the resulting Markov-normalized variable-bandwidth kernel approximates the heat kernel associated with a conformally transformed Riemannian metric whose volume measure has uniform density relative to μ . In other words, the kernel-induced Riemannian geometry “balances out” the sampling distribution of the training data.

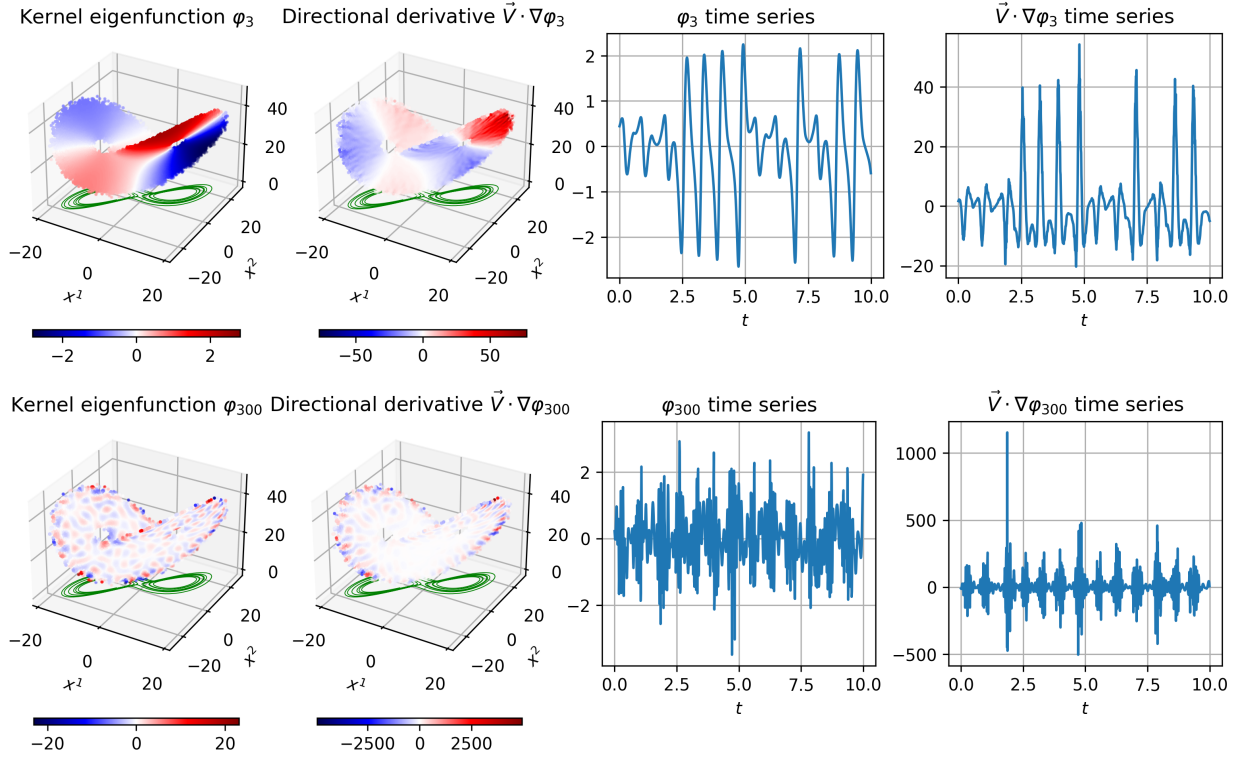


Figure B.8: As in Fig. 2, but for eigenfunctions $\phi_{j,N}$ and directional derivatives $\phi'_{j,N}$ computed using bistochastic Markov normalization of the fixed-bandwidth kernel (B.1). While leading eigenfunctions are qualitatively similar to their variable-bandwidth counterparts (e.g., compare $\phi_{3,N}$ in the top row with the corresponding eigenfunction in Fig. 2), eigenfunctions further down the spectrum become significantly less regular. For example, $\phi_{300,N}$ shown in the bottom row is dominated by “spikes” near the boundary of the attractor where sampling is relatively sparser. The lack of regularity affects the directional derivatives $\phi'_{j,N}$, as manifested by the spiking behavior of the $\phi'_{300,N}$ time series in this example (bottom right panel).

While in many applications μ is not smooth, empirically we find that the variable-bandwidth procedure improves the regularity of numerically computed eigenfunctions. For example, see Fig. 2 and Fig. B.8 for a comparison between kernel eigenfunctions computed on the Lorenz attractor with and without the use of variable-bandwidth kernels. The addition of the variable-bandwidth step leads to considerably smoother eigenfunctions $\phi_{j,N}$ and their directional derivatives under the dynamical vector field, particularly in regions near the boundary of the attractor where sampling is sparse.

For further details on the construction of the kernel (B.2) and the bandwidth tuning algorithm as used in this paper we refer the reader to Appendices A of [20, 46], as well as the code repository accompanying this paper.

References

- [1] V. Baladi, Positive Transfer Operators and Decay of Correlations, Vol. 16 of Advanced Series in Nonlinear Dynamics, World Scientific, Singapore, 2000.
- [2] T. Eisner, B. Farkas, M. Haase, R. Nagel, Operator Theoretic Aspects of Ergodic Theory, Vol. 272 of Graduate Texts in Mathematics, Springer, Cham, 2015.
- [3] G. Froyland, Ulam’s method for random interval maps, Nonlinearity 12 (4) (1999) 1029–1052. doi:10.1088/0951-7715/12/4/318.
- [4] M. Dellnitz, O. Junge, On the approximation of complicated dynamical behavior, SIAM J. Numer. Anal. 36 (1999) 491. doi:10.1137/S0036142996313002.

- [5] I. Mezić, Spectral properties of dynamical systems, model reduction and decompositions, *Nonlinear Dyn.* 41 (2005) 309–325. doi:10.1007/s11071-005-2824-x.
- [6] S. Klus, F. Nüske, P. Koltai, H. Wu, I. Kevrekidis, C. Schütte, F. Noé, Data-driven model reduction and transfer operator approximation, *J. Nonlinear Sci.* 28 (2018) 985–1010. doi:10.1007/s00332-017-9437-7.
- [7] S. L. Brunton, M. Budisić, E. Kaiser, J. N. Kutz, Modern Koopman theory for dynamical systems, *SIAM Rev.* 64 (2) (2022) 229–340. doi:10.1137/21M1401243.
- [8] S. E. Otto, C. W. Rowley, Koopman operators for estimation and control of dynamical systems, *Annu. Rev. Control Robot. Auton. Syst.* 4 (2021) 59–87. doi:10.1146/annurev-control-071020-010108.
- [9] M. Colbrook, The multiverse of dynamic mode decomposition algorithms, in: *Handbook of Numerical Analysis*, Amsterdam, 2024, p. 88.
- [10] I. Mezić, Analysis of fluid flows via spectral properties of the Koopman operator, *Annu. Rev. Fluid Mech.* 45 (2013) 357–378. doi:10.1146/annurev-fluid-011212-140652.
- [11] G. Froyland, D. Giannakis, B. Lintner, M. Pike, J. Slawinska, Spectral analysis of climate dynamics with operator-theoretic approaches, *Nat. Commun.* 12 (2021). doi:10.1038/s41467-021-26357-x.
- [12] H. Wu, F. Nüske, F. Paul, S. Klus, P. Koltai, F. Noé, Variational Koopman models: Slow collective variables and molecular kinetics from short off-equilibrium simulations, *J. Chem. Phys.* 146 (2017). doi:10.1063/1.4979344.
- [13] Y. Susuki, I. Mezić, F. Raak, T. Hikiyara, Applied Koopman operator theory for power systems technology, *NOLTA* 7 (4) (2016) 430–459. doi:10.1587/nolta.7.430.
- [14] A. Mauroy, I. Mezić, Y. Susuki (Eds.), *The Koopman Operator in Systems and Control*, no. 484 in *Lecture Notes in Control and Information Sciences*, Springer, 2020. doi:10.1007/978-3-030-35713-9.
- [15] P. Walters, *An Introduction to Ergodic Theory*, Vol. 79 of *Graduate Texts in Mathematics*, Springer-Verlag, New York, 1981.
- [16] W. Tucker, The Lorenz attractor exists, *C. R. Acad. Sci. Paris, Ser. I* 328 (1999) 1197–1202.
- [17] S. Luzzatto, I. Melbourne, F. Paccaut, The Lorenz attractor is mixing, *Comm. Math. Phys.* 260 (2) (2005) 393–401.
- [18] M. Raissi, P. Perdikaris, G. E. Karniadakis, Physics-informed neural networks: A deep learning framework for solving forward and inverse problems involving nonlinear partial differential equations, *J. Comput. Phys.* 378 (2019) 686–707. doi:10.1016/j.jcp.2018.10.045.
- [19] P. J. Baddoo, B. Herrmann, B. J. McKeon, J. N. Kutz, S. L. Brunton, Physics-informed dynamic mode decomposition, *Proc. R. Soc. A* 479 (2023). doi:10.1098/rspa.2022.0576.
- [20] S. Das, D. Giannakis, J. Slawinska, Reproducing kernel Hilbert space compactification of unitary evolution groups, *Appl. Comput. Harmon. Anal.* 54 (2021) 75–136. doi:10.1016/j.acha.2021.02.004.
- [21] D. Giannakis, C. Valva, Consistent spectral approximation of Koopman operators using resolvent compactification, *Nonlinearity* 37 (7) (2024). doi:10.1088/1361-6544/ad4ade.
- [22] B. O. Koopman, Hamiltonian systems and transformation in Hilbert space, *Proc. Natl. Acad. Sci.* 17 (5) (1931) 315–318. doi:10.1073/pnas.17.5.315.
- [23] B. O. Koopman, J. von Neumann, Dynamical systems of continuous spectra, *Proc. Natl. Acad. Sci.* 18 (3) (1932) 255–263. doi:10.1073/pnas.18.3.255.
- [24] M. H. Stone, On one-parameter unitary groups in Hilbert space, *Ann. Math* 33 (3) (1932) 643–648. doi:doi.org/10.2307/1968538.
- [25] K. Schmüdgen, *Unbounded Self-Adjoint Operators on Hilbert Space*, Vol. 265 of *Graduate Texts in Mathematics*, Springer Science+Business Media, 2012.
- [26] C. R. de Oliveira, *Intermediate Spectral Theory and Quantum Dynamics*, Vol. 54 of *Progress in Mathematical Physics*, Birkhäuser, Basel, 2009.
- [27] F. Chatelin, *Spectral Approximation of Linear Operators*, *Classics in Applied Mathematics*, Society for Industrial and Applied Mathematics, Philadelphia, 2011.
- [28] B. K. Sriperumbudur, K. Fukumizu, G. R. Lanckriet, Universality, characteristic kernels and RKHS embedding of measures, *J. Mach. Learn. Res.* 12 (2011) 2389–2410.
- [29] R. Coifman, M. Hirn, Bi-stochastic kernels via asymmetric affinity functions, *Appl. Comput. Harmon. Anal.* 35 (1) (2013) 177–180. doi:10.1016/j.acha.2013.01.001.
- [30] V. I. Paulsen, M. Raghupathi, *An Introduction to the Theory of Reproducing Kernel Hilbert Spaces*, Vol. 152 of *Cambridge Studies in Advanced Mathematics*, Cambridge University Press, Cambridge, 2016.
- [31] I. Steinwart, A. Christmann, *Support Vector Machines*, *Information Science and Statistics*, Springer, New York, 2008.
- [32] I. Babuška, J. Osborn, Eigenvalue problems, in: P. G. Ciarlet, J. L. Lions (Eds.), *Finite Element Methods (Part 1)*, Vol. II of *Handbook of Numerical Analysis*, North-Holland, Amsterdam, 1991, pp. 641–787.
- [33] M. Reed, B. Simon, *Methods of Modern Mathematical Physics I: Functional Analysis*, Academic Press, New York, 1980.
- [34] M. Blank, Egodic averaging with and without invariant measures, *Nonlinearity* 30 (2017) 4649–4664. doi:10.1088/1361-6544/aa8fe8.
- [35] U. von Luxburg, M. Belkin, O. Bousquet, Consistency of spectral clustering, *Ann. Stat.* 26 (2) (2008) 555–586. doi:10.1214/009053607000000640.
- [36] J. C. Oxtoby, Stepanoff flows on the torus, *Proc. Amer. Math. Soc.* 4 (1953) 982–987.
- [37] E. N. Lorenz, Deterministic nonperiodic flow, *J. Atmos. Sci.* 20 (1963) 130–141. doi:10.1175/1520-0469(1963)020<0130:DNF>2.0.CO;2.
- [38] A. Katok, J.-P. Thouvenot, Spectral properties and combinatorial constructions in ergodic theory, in: B. Hasselblatt, A. Katok (Eds.), *Handbook of Dynamical Systems*, Vol. 1B, North-Holland, Amsterdam, 2006, Ch. 11, pp. 649–743.
- [39] A. V. Kočergin, Time changes in flows and mixing, *Math. USSR Izv.* 7 (6) (1973) 1273–1294. doi:10.1070/

IM1973v007n06ABEH002087.

- [40] B. Fayad, Analytic mixing reparametrizations of irrational flows, *Ergod. Th. & Dynam. Sys.* 22 (2002) 437–468. doi:10.1017/s0143385702000214.
- [41] K. Law, A. Shukla, A. M. Stuart, Analysis of the 3DVAR filter for the partially observed Lorenz’63 model, *Discrete Contin. Dyn. Syst.* 34 (3) (2013) 1061–10178. doi:10.3934/dcds.2014.34.1061.
- [42] J. C. Sprott, *Chaos and Time-Series Analysis*, Oxford University Press, Oxford, 2003.
- [43] M. Korda, M. Putinar, I. Mezić, Data-driven spectral analysis of the Koopman operator, *Appl. Comput. Harmon. Anal.* 48 (2) (2020) 599–629. doi:10.1016/j.acha.2018.08.002.
- [44] M. J. Colbrook, C. Drysdale, A. Horning, Rigged Dynamic Mode Decomposition: Data-driven generalized eigenfunction decompositions for Koopman operators (2024).
URL <https://arxiv.org/abs/2405.00782>
- [45] M. J. Colbrook, I. Mezić, A. Stepanenko, Limits and Powers of Koopman Learning, arXiv:2407.06312 [math] (Jul. 2024).
doi:10.48550/arXiv.2407.06312.
URL <http://arxiv.org/abs/2407.06312>
- [46] D. Giannakis, Data-driven spectral decomposition and forecasting of ergodic dynamical systems, *Appl. Comput. Harmon. Anal.* 47 (2) (2019) 338–396. doi:10.1016/j.acha.2017.09.001.
- [47] G. B. Folland, *A Course in Abstract Harmonic Analysis*, Chapman and Hall/CRC, 2016. doi:10.1201/b19172.
- [48] T. Berry, J. Harlim, Variable bandwidth diffusion kernels, *Appl. Comput. Harmon. Anal.* 40 (1) (2016) 68–96. doi:10.1016/j.acha.2015.01.001.
- [49] R. R. Coifman, S. Lafon, Diffusion maps, *Appl. Comput. Harmon. Anal.* 21 (2006) 5–30. doi:10.1016/j.acha.2006.04.006.
- [50] R. R. Coifman, Y. Shkolnisky, F. J. Sigworth, A. Singer, Graph Laplacian tomography from unknown random projections, *IEEE Trans. Image Process.* 17 (10) (2008) 1891–1899. doi:10.1109/tip.2008.2002305.